⌘ Author's Choice

A Chemical Proteomics Approach to Profiling the ATP-binding Proteome of *Mycobacterium tuberculosis**

Lisa M. Wolfe,[a] Usha Veeraraghavan,[b] Susan Idicula-Thomas,[c,d,e] Stephan Schürer,[c,f,g] Krister Wennerberg,[h] Robert Reynolds,[i] Gurdyal S. Besra,[b] and Karen M. Dobos[a,j]

Tuberculosis, caused by *Mycobacterium tuberculosis*, remains one of the leading causes of death worldwide despite extensive research, directly observed therapy using multidrug regimens, and the widespread use of a vaccine. The majority of patients harbor the bacterium in a state of metabolic dormancy. New drugs with novel modes of action are needed to target essential metabolic pathways in *M. tuberculosis*; ATP-competitive enzyme inhibitors are one such class. Previous screening efforts for ATP-competitive enzyme inhibitors identified several classes of lead compounds that demonstrated potent anti-mycobacterial efficacy as well as tolerable levels of toxicity in cell culture. In this report, a probe-based chemoproteomic approach was used to selectively profile the *M. tuberculosis* ATP-binding proteome in normally growing and hypoxic *M. tuberculosis.* From these studies, 122 ATP-binding proteins were identified in either metabolic state, and roughly 60% of these are reported to be essential for survival *in vitro*. These data are available through ProteomeXchange with identifier PXD000141. Protein families vital to the survival of the tubercle bacillus during hypoxia emerged from our studies. Specifically, along with members of the DosR regulon, several proteins involved in energy metabolism (Icl/Rv0468 and Mdh/Rv1240) and lipid biosynthesis (UmaA/Rv0469, DesA1/Rv0824c, and DesA2/Rv1094) were found to be differentially abundant in hypoxic *versus* normal growing cultures. These pathways represent a subset of proteins that may be relevant therapeutic targets for development of novel ATP-competitive antibiotics. ***Molecular & Cellular Proteomics 12: 10.1074/mcp.M112.025635, 1644–1660, 2013.***

Tuberculosis remains a significant global health burden, and the emergence of multidrug-resistant and extensively drug-resistant cases continue to increase (1). Thus novel chemotherapeutics for the treatment of drug-resistant disease are needed. In addition, antibiotics that reduce the effective time (>6 months) and complexity of antibiotic regimens used (three to four drugs in tandem) are needed for more effective treatment of *Mycobacterium tuberculosis*. The recent description of ATP-competitive enzyme inhibitors as a novel class of antitubercular drugs (2–5) has bolstered interest in the identification of bacterial enzymes that utilize ATP as these enzymes may be essential and druggable targets for the discovery and design of such small molecule inhibitors. Furthermore, elucidating ATP-dependent catalytic pathways present in differing metabolic disease states is critical for understanding mechanisms of latency, virulence, and pathogenesis. This study and others (6) lay the groundwork for profiling of the ATPome across diverse infectious diseases under different metabolic states that may be relevant within the host milieu, with the goal of identifying critical and potentially druggable ATP-dependent pathways. For noninfectious diseases, a recent study utilized activity-based chemoproteomic profiling in murine models of induced obesity to study metabolic changes associated with mitochondrial dysfunction (7). For *M. tuberculosis*, manipulation of these critical signaling pathways via novel chemotherapeutic strategies could not only increase the effectiveness of drug treatment in multidrug-resistant/extensively drug-resistant cases but may also enhance efficacy *in vivo* against bacilli exhibiting multiple and often resistant phenotypes within the host (8).

The study of kinases and other ATP-binding proteins (chaperones, ATPases, synthases, and other metabolic enzymes) has become important in elucidating the roles of ATP-dependent pathways in the pathogenesis of cancer and other mechanisms of dysregulated growth. The large scale profiling

From the [a]Department of Microbiology, Immunology, and Pathology, Colorado State University, Fort Collins, Colorado, 80523, the [b]School of Biosciences, College of Life and Environmental Sciences, University of Birmingham, Edgbaston, Birmingham, B15, United Kingdom, the [c]Center for Computational Science, University of Miami, Miami, Florida, 33136, the [d]Biomedical Informatics Center, National Institute for Research in Reproductive Health, Indian Council of Medical Research, Mumbai, India, 400012, the [f]Department of Pharmacology, Miller School of Medicine, University of Miami, Miami, Florida, 33136, the [h]Institute for Molecular Medicine Finland, University of Helsinki, Helsinki, Finland, 00100, and the [i]Department of Chemistry, College of Arts and Sciences, University of Alabama at Birmingham, Birmingham, Alabama, 35205

Received November 15, 2012, and in revised form, February 26, 2013

⌘ *Author's Choice*—Final version full access.

Published, MCP Papers in Press, March 5, 2013, DOI 10.1074/mcp.M112.025635

of such networks is facilitated with the use of active-site nucleotide capture probes (9, 10). Traditionally, studies have utilized this chemical proteomics approach to map cellular interaction networks of protein kinase inhibitors as well as to elucidate global protein kinase profiles of cell lines (10–12). Here, we describe a chemical proteomics method that is designed to capture the full array of adenosine nucleotide-binding proteins, or the ATPome, of *M. tuberculosis* H_{37}Rv. This method utilizes a desthiobiotin-conjugated ATP as a molecular probe in which target enzymes are covalently modified with biotin within characteristic active sites, in this case the nucleotide binding domains of kinases and other ATP-binding proteins. Once labeled, ATP-binding proteins are subsequently digested with trypsin and labeled peptides enriched via streptavidin affinity capture beads and subjected to LC-MS/MS for the identification of ATP-labeled proteins. The utility of this approach is multifaceted; the profiling of inhibitor selectivity in native proteomes can be achieved quickly and without the need for radiolabeling, recombinant enzymes, and functional assays. Additionally, the differential abundances of ATP-binding proteins during different growth states and conditions can be selectively monitored and quantified. Thus, this technology can be broadly applied to emerging infectious diseases and/or select agents where few other tools are readily available for drug discovery. Here, we identified essential gene products critical to survival, adaptation, and the development of drug resistance in *M. tuberculosis*. These results may lead to the identification and facile monitoring of novel therapeutic targets and their interactions within pathogen-specific pathways.

EXPERIMENTAL PROCEDURES

Bacterial Growth—M. tuberculosis, H_{37}Rv seed culture was grown to log phase (A_{600} 1.2) in Middlebrook 7H9, ADC. Normally grown cultures were as follows. Three cultures (195 ml in 500-ml vented cap flasks) were inoculated with 2.5 ml of seed culture. A magnetic stir bar was added, and cultures were incubated at 37°C with stirring (200 rpm) to a final A_{600} 1.2–1.6. For hypoxic cultures, six cultures (paired replicates of 390 ml in 500-ml sealed cap flasks) were inoculated with 5.0 ml of seed culture. Cultures were incubated at 37°C with stirring (100 rpm) to a final A_{600} 0.65–0.70. Cell pellets were harvested on days 7 (normal) and 14 (hypoxic).

Sample Preparation—Cell pellets were resuspended at a concentration of 0.5 g/ml in IP/Lysis Buffer (25 mM Tris-HCl, pH 7.4, 150 mM NaCl, 1 mM EDTA, 1% Nonidet P-40, and 5% glycerol) containing HALT™ protease/phosphatase inhibitor mixture (ThermoPierce). Resuspended cells were placed in Lysing Matrix B bead beater vials (pre-filled with 0.1 mm of silica; MP Biomedicals). Lysis of cells occurred over 12 bead-beat cycles (30 s lyse/45 s rest on ice). Cell lysates were cleared of silica and cellular debris via centrifugation at 4,000 × *g* for 10 min. Supernatant was transferred to a new microcentrifuge tube and centrifuged again for 10 min at 13,000 × *g*. Cleared lysate was then filtered through a 0.8/0.2-μm syringe filter to sterilize the lysate for working under BSL-2 conditions. The sterile lysate was desalted using 7K Thermo Scientific Zeba™ spin desalting columns, and the protein amount was quantified by BCA (ThermoPierce). 500-μg aliquots of whole cell lysate were labeled with 5 mM desthiobiotin-ATP for 10 min as per the manufacturer's instructions (ThermoPierce).

Active Site Peptide Capture—Desthiobiotin-ATP-labeled proteins were reduced in 1 mM DTT and alkylated in 1 mM iodoacetamide before buffer exchange into digestion buffer (20 mM Tris, pH 8.0, 2 M urea). Each sample was digested with trypsin (1 μg/μl) at an enzyme to substrate ratio of 1:50 for 2 h at 37°C. Peptide capture with streptavidin-agarose resin and elution using 50% acetonitrile, 0.1% TFA was followed as per the manufacturer's instructions.

LC-MS—Peptides were separated on a nanospray column (Zorbax 300SB-C18, 3.5 μm, 75-μm inner diameter × 150-mm column (Agilent Technologies)). Samples were eluted into an LTQ linear ion trap mass spectrometer (Thermo Fisher Scientific) using a gradient of 0–100% B (A = 3% ACN, 0.1% formic acid; B = 100% ACN, 0.1% formic acid) at a flow rate of 300 nl/min for 103 min. All samples were run in triplicate.

Database Searching—Tandem mass spectra were extracted, charge state deconvoluted, and deisotoped by Xcalibur version 2.2 SP1. All MS/MS samples were analyzed using Mascot (Matrix Science, London, UK; version 2.3.02) and SEQUEST (Thermo Fisher Scientific, San Jose, CA; version v.27, revision 11). Mascot and SEQUEST were set up to search the MtbReverse041712 database (7992 entries) assuming the digestion enzyme trypsin. Parameters for both search engines were set to a fragment ion mass tolerance of 1.0 Da and a parent ion tolerance of 2.5 Da. Oxidation of methionine, iodoacetamide derivative of cysteine, and the desthiobiotin modification of lysine were specified in Mascot and SEQUEST as variable modifications.

Criteria for Protein Identification—Scaffold (version Scaffold_3.6.1, Proteome Software Inc., Portland, OR) was used to validate MS/MS-based peptide and protein identifications. Peptide identifications were accepted if they exceeded specific database search engine thresholds. Mascot identifications required ion scores to be greater than the associated identity scores and 50, 65, 65, and 65 for singly, doubly, triply, and quadruply charged peptides. SEQUEST identifications required Δ*Cn* scores of greater than 0.2 and XCorr scores of greater than 1.8, 2.0, 3.0, and 4.0 for singly, doubly, triply, and quadruply charged peptides. Protein identifications were accepted if they contained at least one identified peptide in at least two biological replicates. Peptide spectra meeting the most minimum requirements were manually inspected for quality, using metrics described previously (13, 14). Quantification of proteins was performed on normalized spectral abundance factors for each protein (NSAF)[1] (13–15). Proteins that contained similar peptides and could not be differentiated based on MS/MS analysis alone were grouped to satisfy the principles of parsimony. False discovery rates were calculated for each reported data set as follows: hypoxic *versus* normal (FDR = 13.1%), normal_ATP *versus* normal_ATPγS (FDR = 3.2%), hypoxic_ATP *versus* hypoxic_ATPγS (FDR = 11.2%), and the noncomparative ATPome (FDR = 6%). The mass spectrometry proteomics data have been deposited in the ProteomeXchange Consortium via the PRIDE partner repository (16) with the dataset identifier PXD000141.

Statistical Analysis—The design for each experimental condition consisted of three biological replicates per sample group (normal/hypoxic-ATP, normal/hypoxic-ATPγS, and normal/hypoxic-streptavidin only). In the case of hypoxic cultures, six biological replicates were grown to set time points, and cell material was pooled into three-paired replicates and subsequently treated as triplicate replications.

[1] The abbreviations used are: NSAF, normalized spectral abundance factor; ATPγS, adenosine 5′-[γ-thio]triphosphate tetralithium; BisTris, 2-[bis(2-hydroxyethyl)amino]-2-(hydroxymethyl)propane-1,3-diol; FC, fold change; USP, universal stress protein; FDR, false discovery rate; Icl, isocitrate lyase; STPK, serine/threonine kinase.

Each replicate was injected into the mass spectrometer three times for a total of nine injections per sample. Spectral count data, as visualized in Scaffold (Proteome software, version 3.6.1), were normalized to quantitative values using normalized spectral abundance factors, as described previously (13–15). Statistical analysis was performed using Fisher's exact test in the comparison of two groups (*i.e.* normal-ATP *versus* hypoxic-ATP or normal-ATP *versus* normal-ATPγS). Fisher's exact test is a valid method of identifying differences in protein abundance (*i.e.* spectral counts) in shotgun proteomics data sets using experimental designs of at least three biological replicates, and it performs with similar power to more complex generalized linear modeling strategies (17).

Blast-based Sequence Description—The most relevant description for each of the sequences was acquired based on the significant BLAST results. The homologs for the sequences were retrieved using the Blastp algorithm and the nonredundant database of NCBI. The Blast2GO suite (18) was used for this purpose, because it can annotate several sequences in one session.

Gene Ontology Annotation—The Pfam domains were mapped to Gene Ontology (GO) terms using the lookup table provided by Pfam2go. GO terms are hierarchical and inter-related in nature. All the GO terms originate from three distinct subsumption hierarchy trees, namely cellular component, biological process, and molecular function. Thus, each domain can have multiple GO terms based on the level and type of annotation. An in-house script was written to retrieve GO annotations based on the root term "molecular function" and their distance from the root term.

PFAM Domain-based Annotation—The InterPro and Pfam IDs corresponding to the GO term "ATP binding" (GO ID:0005524) were retrieved using the QuickGO and InterPro BioMart web services. The ATP binding associated domains were queried against the ATP-binding proteome data sets according to spectral quality (high, medium, and low confidence). Their Pfam and InterPro descriptions were identified using the InterProscan web service, which was accessed via the Pipeline Pilot (Accelrys) implementation in the sequence analysis collection. Mapping the domain and the labeled peptide sequences retained the information for the relevant domains.

Immunoblots—5 μg of normal and hypoxic lysates were separated on 4–12% BisTris SDS-polyacrylamide gel (Invitrogen). Primary antibodies were either mouse monoclonal (HspX, Ald, Hbha, GlcB, and KatG) or rabbit polyclonal (Rv0569, Rv1738, Rv2626c, Rv2032, and Rv3133c) and diluted to suggested titers. The monoclonal antibody against Hbha was provided as a kind gift from Dr. Mike Brennan (Food and Drug Administration, Silver Spring, MD); the polyclonal antibody against Rv3133 and recombinant protein Rv3133 were provided as kind gifts from Dr. David Sherman (Seattle Biomedical Research Institute, Seattle, WA). The rabbit polyclonal antibodies against Rv0569, Rv1738, Rv2626, and Rv2032 were made by subcutaneous injection of 0.5 mg of recombinant antigen in an emulsion with Complete Freund's adjuvant, followed by two additional injections of 0.5 mg of antigen in an emulsion with Incomplete Freund's adjuvant 21 and 42 days after the initial injection. The recombinant antigens Rv0569 and Rv2626c were made via expression and purification from recombinant clones as described previously (13), and the expression and purification of recombinant Rv1738 and Rv2032 followed methods analogous to that used for recombinant Rv2626c. All antibodies and recombinant clones, with the exception of anti-Rv3133, are available through BEI Resources. Control samples consisted of recombinant proteins generated from *E. coli* or, if unavailable, whole cell lysate from *M. tuberculosis,* H_{37}Rv (Hbha, KatG, Ald). Protein bands were visualized via alkaline phosphatase-conjugated IgG (Sigma-Aldrich). Densitometry analysis was performed via the ImageJ suite (rsbweb.nih.gov).

RESULTS

M. tuberculosis ATPome—A shotgun proteomics analysis was performed on the enriched subproteome of desthiobiotin-labeled ATP-binding proteins (ATPome). We identified a total of 176 proteins, of which 122 (69%) were labeled via the nucleotide probe, validating the approach for rapid identification of a crucial and potentially druggable subclass of the *M. tuberculosis* proteome (supplemental Table S1). Selective labeling was further validated by ranking the tagged proteins using a metric of ATP labeling based on protein and peptide confidence levels greater than 90% as well as manual interpretation of spectral quality for each peptide sequence labeled with a desthiobiotin tag (19). This ranking accounted for the variation among identified peptides in signal to noise levels and sequence coverage. Proteins were listed by the quality of spectra demonstrating a desthiobiotin-labeled lysine (differential modification of lysine of +196 Da). Low confidence peptide spectra exhibited no less than 90% peptide confidence with a minimum of one assigned peptide (number identified was 21; supplemental Tables S1, S2, and S6). Medium confidence peptide spectra had a peptide score between 90 and 95% with two or more assigned peptides (number identified was 20; supplemental Tables S1 and S2). Proteins determined to have labeling in the high confidence range exhibited greater than 95% peptide confidence and had two or more unique peptides assigned for identification (number identified was 81; supplemental Tables S1 and S2). A no-probe, streptavidin-only control was performed to account for proteins that have inherent biotin-like domains and may nonspecifically interact with the streptavidin capture resin. Results from the control experiments revealed that only a few proteins, GroEL2 (Rv0440), DnaK (Rv0350), and HspX (Rv2031c), the acyl-carrier protein AcpM (Rv2244), peptidyl-prolyl *cis-trans* isomerase PpiA (Rv0009), and the naturally biotinylated acetyl carboxylase AccA3 (Rv3285), bound streptavidin nonspecifically in addition to being confidently labeled with the desthiobiotin probe. In the case of GroEL2, DnaK, and HspX, we believe the promiscuous binding to the affinity resin was due to the high abundance of each protein and their chaperoning function. PpiA, although not present in high abundance, also aids in protein folding and thus may associate with the other identified chaperones (20). AccA3 most likely bound the molecular probe (and thus the streptavidin capture resin) by virtue of its affinity for biotin and biotin-like molecules (21). AcpM is functionally associated with AccA3 as both proteins are involved in long chain fatty acid synthesis. Their association in this pathway is visualized via the STRING database (version 9.0 2012 (22)), with curated pathway interactions in the BioCyc version 16.1 pathway collection, and thus may explain the identification of AcpM in this control group. Overall, the utilization of the active site nucleotide probe to capture ATP-binding proteins resulted in

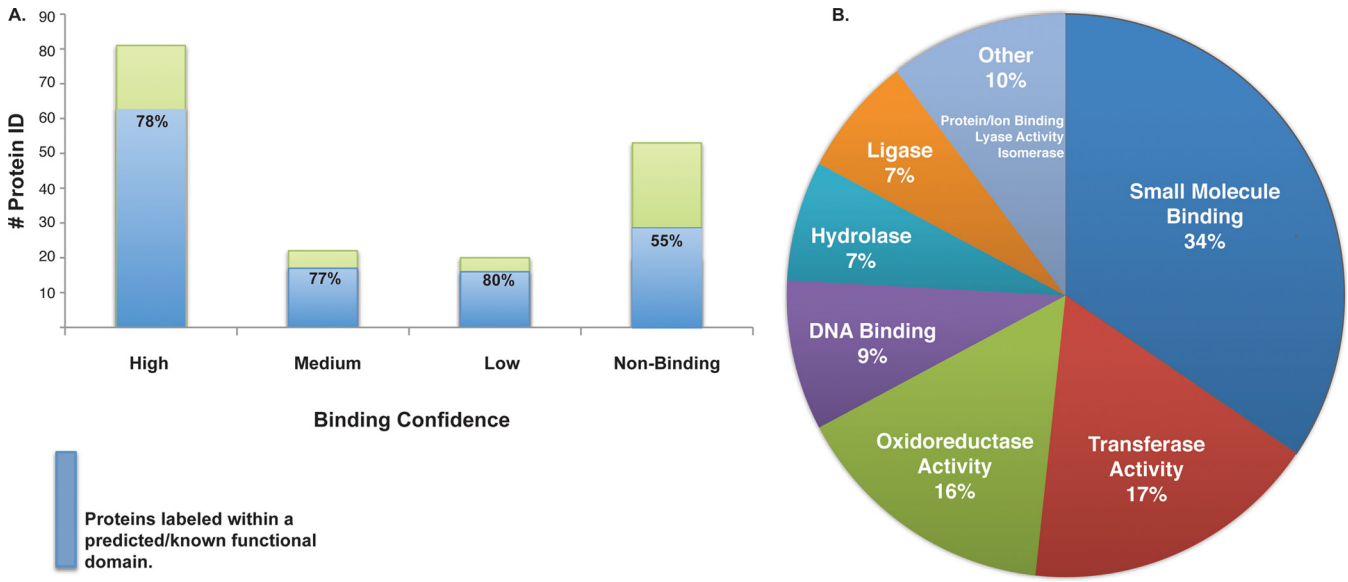

FIG. 1. **Primary sequence analysis of ATP-binding peptides and proteins.** Each protein sequence was submitted for *in silico* analysis through InterPro and sorted via Gene Ontology (molecular function). *A,* approximately 80% of the ATP-binding (*i.e.* desthiobiotin-labeled) proteins could be mapped to Pfam domains. Binding confidence, high, medium, and low, was empirically determined associated with the quality of labeled peptide spectra (*i.e.* confident sequence coverage and low signal to noise). *B,* functions of small molecule binding, transferase, and oxidoreductase activity described the majority of ATPome enzymatic properties.

a highly enriched subproteome of essential and potentially druggable targets.

Functional Annotation of Labeled Proteins—Over half (59%) of the proteins within the identified *M. tuberculosis* ATPome harbor essential functions to support growth (23, 24), indicating that the *M. tuberculosis* ATPome in general is functionally important. A list of all identified proteins and their annotation as essential or nonessential for *in vitro* growth is provided in supplemental Table S1. Functional annotation of the proteins was conducted to identify the functional domains and domain families that were selectively labeled and enriched via our chemical proteomic techniques. In total, 218 protein domain families (Pfams) were associated with the GO term ATP binding (GO ID:0005524). The amino acid sequence of each identified protein and covalently labeled peptide sequence was subjected to an InterPro pattern search to identify functional domains and associate these regions within the list 218 annotated domain families (Pfams) (25). It was determined that 13 ATP-associated Pfams were represented in the ATPome dataset across all ranges of labeling confidence (low to high, $n = 122$), and none were represented in proteins identified but not labeled with nucleotide probe ($n = 54$) (supplemental document S1). Among the ATP-associated Pfams were proteins involved with ATP synthesis (PF00006) and peptidoglycan synthesis (Mur Ligase (PF01225)), as well as protein kinases (PF00069). Overall, ~80% of the ATPome had peptides that could be mapped to Pfam domains (Fig. 1*A*). The majority of enzyme functions identified were associated with the following activities: small molecule binding (34%), transferase (17%), and oxidoreductase (16%) (Fig.1*B*).

To further define the functional classes of proteins within the experimental ATPome dataset, a predictive list of potential ATP-binding proteins was generated by query of the search term ATP-binding in The Tuberculosis Database and was combined with a list of proteins from another web-based resource PATRIC (supplemental Table S7) (26, 27). By functional class, categorization of the predicted *M. tuberculosis* ATP-binding proteome revealed that proteins associated with Category 7 (Intermediary Metabolism) and Category 2 (Information Pathways) were equally represented at 20% and that Category 3 (Cell Wall and Processes) represented ~30% of the predicted subset. When compared with the experimentally derived ATPome subset, 30% of the proteins belong to Category 7, whereas Category 1 (Lipid Metabolism) and Category 10 (Conserved Hypotheticals) represent a collective 33% of the enriched experimental ATPome (Fig. 2). Proteins involved in fatty acid and mycolic acid biosynthesis (Category 1) are of interest due to their key roles in the maintenance of the cell envelope architecture and the essentiality of their encoding genes (24). A complete list of labeled and unlabeled protein IDs and their corresponding functional categories is provided in supplemental Table S1.

Differential Abundance of Proteins in Normoxic (Normal) Versus Hypoxic State Bacteria—The strength of this proteomics approach is the ease with which a crucial and druggable slice of the proteome, the ATPome, can be captured and identified over a variety of time points and metabolic states, particularly the so-called "latent " state of *M. tuberculosis* that is associated with drug resistance. Hence, we utilized the active site nucleotide probes to selectively capture and enrich

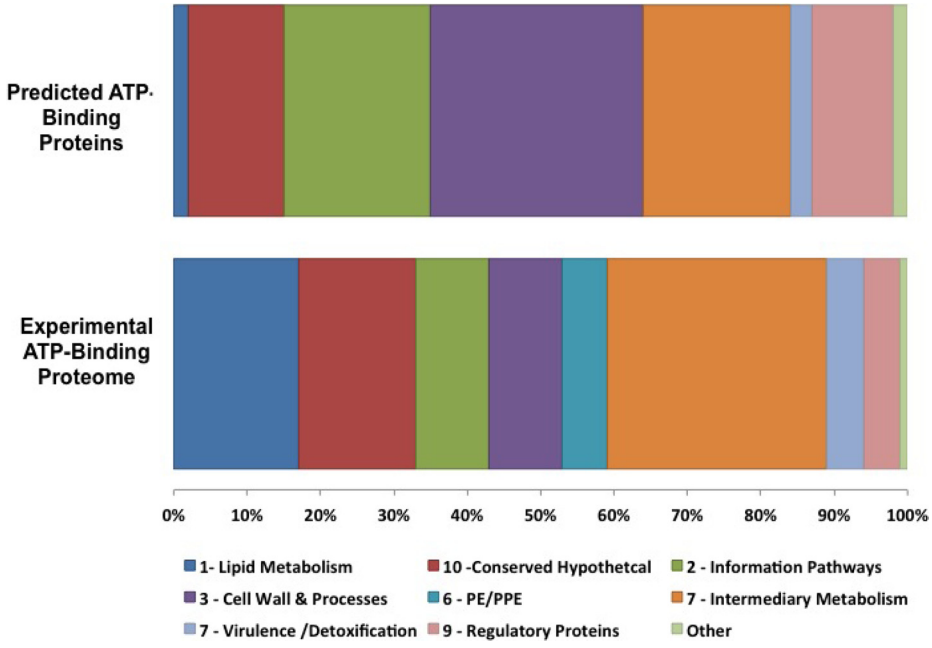

FIG. 2. **Distribution of predicted and experimentally derived ATP-binding proteins by functional category.** A predicted list of ATP-binding proteins was generated from two resources and sorted by functional category. A comparison between the predicted and experimentally derived ATPome demonstrates a range of distribution among each functional category. Representing nearly 50% of the experimental ATPome were proteins within functional Category 7, Intermediary Metabolism, and functional Category 2, Lipid Metabolism. Conserved Hypotheticals (functional Category 10) were the third most represented group.

for the *M. tuberculosis* ATPome under different growth conditions. Normoxic cells growing under standard conditions with aeration and cells grown in limited oxygen conditions (see under "Experimental Procedures"), were harvested, lysed, labeled, and subjected to LC-MS for comparison of their subproteomes (supplemental Table S3). Analysis of NSAF (26, 28) identified 61 differentially abundant proteins based on protein abundance changes that had a *p* value less than 0.05 (19, 29). The log fold change (log FC) values were plotted against the calculated *p* values to visualize the distribution of proteins between the two growth states (Fig. 3). Proteins were determined to be differentially abundant if the calculated log FC was equal to or greater than 1 for proteins with higher abundance in normal samples (Table I) *versus* negative log FC values for proteins in higher abundance during hypoxic growth (Table II). Patterns of protein function within the captured mycobacterial ATPome demonstrate dynamic changes between normal and hypoxic growth and were seen in the Functional Categories 2, 3, 9, and 10. Categories 0, 1, and 7 remain relatively stable (Fig. 4).

During dormancy and hypoxic growth, *M. tuberculosis* undergoes changes in gene expression that typically involve the up-regulation of enzymes involved in alternative metabolic pathways (*i.e.* glyoxylate bypass) and those observed to be under the control of the dormancy regulon *DosR*. The list of proteins in Table II includes the gene products HspX (Rv2031), Acg (Rv2032c), TB31.7 (Rv2623), Rv2624c, and Rv1738. These proteins are directly regulated or co-expressed with the response regulator DosR (Rv3133c) (30).

Isocitrate lyase (Icl, Rv0467), the enzyme that catalyzes the reversible cleavage of isocitrate to glyoxylate and succinate (31) and has a role in the growth, survival, and persistence of *M. tuberculosis* in macrophages and mice (32), was found to be labeled with desthiobiotin-ATP on Lys-322 (PFAM, PF00463) and differentially abundant during hypoxic growth. The second enzyme involved in the glyoxylate cycle, malate synthase G (GlcB, Rv1837c), was also labeled with our active site probe; however, in this study its differential abundance in hypoxically grown cultures was not significant (*p* value $>$ 0.60). We did, however, confirm increased protein levels of GlcB via Western blot (Fig. 5 and supplemental Fig. S1). It is well known that the expression of alanine dehydrogenase (*ald, Rv2780*) is also up-regulated during the growth of *M. tuberculosis* under low oxygen conditions (31). It has recently been shown in *M. tuberculosis* and previously in *Mycobacterium smegmatis* that alanine dehydrogenase is responsible for both glycine and alanine dehydrogenase activities (33, 34). The main role of Ald is to generate L-alanine for peptidoglycan and protein synthesis (33). Both Icl and Ald are unique to bacteria and have no human homologs, making them attractive drug targets. Although no inhibitors for Ald have been reported, Icl inhibitors against dormant and logarithmically grown mycobacteria include the 3-nitropropionamides and 5-nitro-2-furoic acid hydrazones (35). Immunoblots of several proteins found to be in higher abundance during hypoxia confirmed the differences in protein levels found via NSAF for differential quantification (Fig. 5 and supplemental Fig. S1).

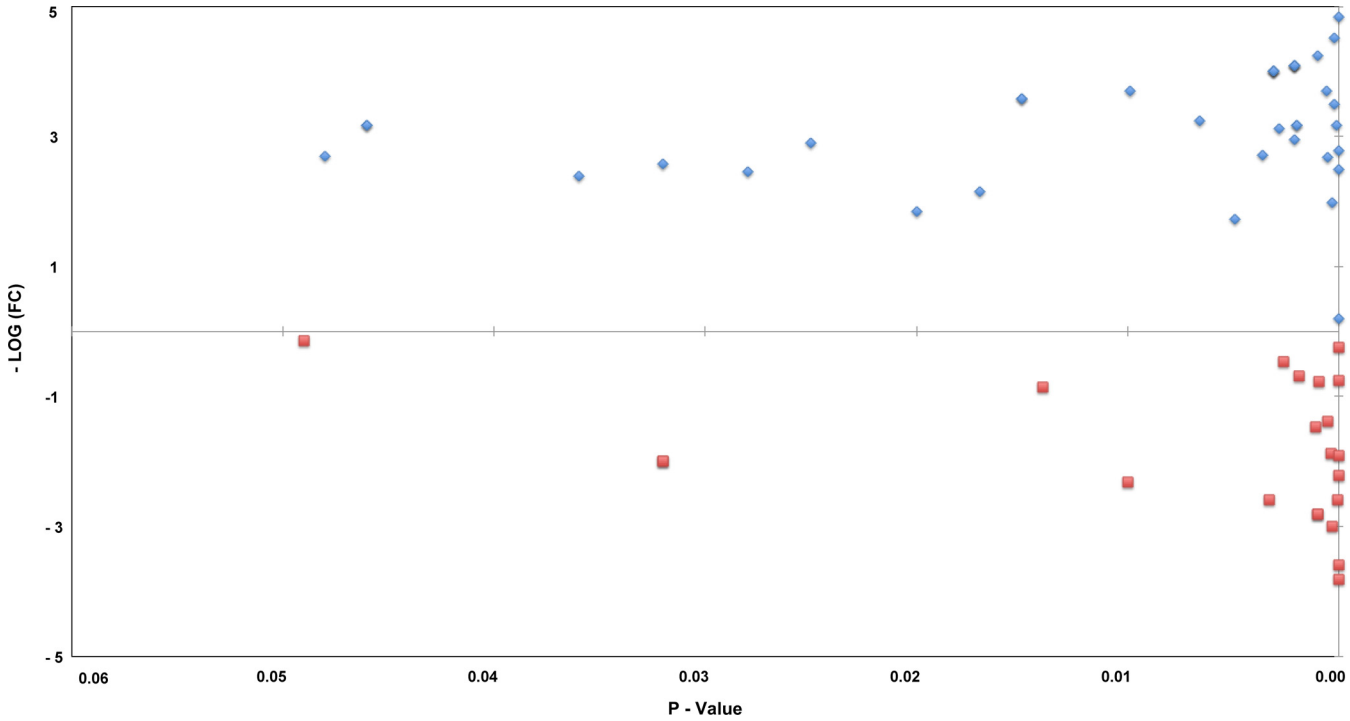

FIG. 3. **Volcano plot of differentially abundant proteins between normal and hypoxic cultures.** Proteins with a positive log fold change (*FC*) were the most differential in normal cultures and are visualized in the *upper half* of the plot. Proteins with a negative log fold change (*FC*) were most differential in hypoxic cultures and are distributed in the *lower half*.

The mycobacterial serine/threonine kinases (STPK) mediate signal transduction among a variety of intra- and extracellular targets (36, 37). We identified six of the 11 STPK gene products, PknABDHEF. Notably, during normal growth we see an increased abundance in labeled PknD (Rv0931c), PknE (Rv1743), and PknH (Rv1266c). The essential STPK PknA was not found to be differentially abundant between the two growth states (logic ~0), whereas PknB was exclusively identified in normally growing cells (data not shown). In addition, several metabolic kinases such as phosphoglycerate kinase Pgk (Rv1743) and the polyphosphate kinase Ppc (Rv2984) were also shown to be more abundant during normal growth (Table I). Aside from PknA and the phosphofructokinase PfkA (Rv3010c) (Table II), the overall lack of protein kinases during dormancy suggests that targeting these proteins under differing metabolic states may not be an efficient means of antimycobacterial killing.

ATP Binding Properties of the M. tuberculosis ATPome—In addition to describing the use of ATP by essential enzymes in the bacterial proteome and identifying those proteins that demonstrated differential abundance patterns between normal and hypoxic states of growth, the third and final goal of this work was to characterize proteins whose ATP-binding function may be utilized in the development of novel ATP-competitive antibiotics. The desthiobiotin labeling of active sites has been used to analyze cellular effects and target selectivity of kinase inhibitors that are clinically approved in the treatment of cancer. In these studies, the binding of the nucleotide probe is quantified in the presence or absence of the drug of choice. These experiments operate under the assumption that for a specific compound-target interaction, the ATP-competitive inhibitor compound will out-compete the binding of the nucleotide probe. As a first step in using this approach to identify native targets of ATP-competitive inhibitors, proteins under both normal oxygen and hypoxic growth conditions were labeled in the presence of excess ATP (ATPγS). ATPγS is a nonhydrolyzable analog of ATP. As the binding of ATP to various protein subunits and active sites can be very dynamic, it has been advantageous to utilize nonhydrolyzable ATP analogs to identify true ATP-binding states of proteins (38). Using this approach, two different sets of proteins were identified as follows: those that bind ATP transiently (*i.e.* the binding of ATPγS and the binding of desthiobiotin-ATP are interchangeable) and proteins for which ATP binding was stable and competitive (*i.e.* proteins that have a significantly reduced capacity to bind the nucleotide probe in the presence of excess ATPγS) (supplemental Tables S4 and S5). The relative abundance profiles for these two sets of proteins are exemplified using data from bacilli grown under normal conditions for DevR and ClpC1, respectively (Fig. 6).

Desthiobiotin-labeled peptides were quantified, and those proteins found to have significant fold change differences between samples labeled in the presence or absence of excess ATPγS are listed in Tables III (hypoxic) and IV (normoxic). From this analysis, most proteins demonstrated similar ATP binding characteristics (transient or competitive), regardless

TABLE I
Proteins with increased abundance during normal growth

Identified proteins	Accession no.	Molecular mass	Fisher's exact test (*p* value)	Normal NSAF	Hypoxic NSAF[a]	Log fold change
Polyphosphate kinase, Ppk	Rv2984	83 kDa	(0.0000)	66	1	6.04
Phosphoglycerate kinase, Pgk	Rv1437	43 kDa	(0.0000)	57	2	4.83
Acyl-CoA dehydrogenase, FadE4	Rv0231	63 kDa	(0.0002)	23	1	4.52
Dehydrogenase	Rv3389c	30 kDa	(0.0010)	19	1	4.25
19-kDa lipoprotein antigen precursor, LpqH	Rv3763	15 kDa	(0.0021)	17	1	4.09
Immunogenic protein, Mpt64	Rv1980c	25 kDa	(0.0021)	17	1	4.09
Hypothetical protein	Rv2319c	32 kDa	(0.0021)	17	1	4.09
Aminomethyltransferase, GcvT	Rv2211c	40 kDa	(0.0021)	17	1	4.09
Superoxide dismutase soda	Rv3846	23 kDa	(0.0031)	16	1	4.00
Cysteinyl-tRNA synthetase 1, CysS1	Rv3580c	52 kDa	(0.0031)	16	1	4.00
DNA polymerase I, PolA	Rv1629	98 kDa	(0.0031)	16	1	4.00
Transmembrane serine/threonine-protein kinase E, PknE	Rv1743	61 kDa	(0.0031)	16	1	4.00
Iron-regulated short-chain dehydrogenase/reductase	Rv3224	30 kDa	(0.0006)	26	2	3.70
Fatty-acid-CoA ligase, FadD23	Rv3826	63 kDa	(0.0099)	13	1	3.70
Leucyl-tRNA synthetase, LeuS	Rv0041	108 kDa	(0.0150)	12	1	3.58
Pyridoxamine 5-phosphate oxidase, PdxH	Rv2607	25 kDa	(0.0150)	12	1	3.58
Conserved hypothetical protein	Rv2624c	29 kDa	(0.0002)	34	3	3.50
Aldehyde dehydrogenase	Rv0458	55 kDa	(0.0066)	19	2	3.25
Acetyl-/propionyl-CoA carboxylase α subunit, AccA1	Rv2501c	71 kDa	(0.0001)	45	5	3.17
Fatty-acid-CoA ligase, FadD7	Rv0119	55 kDa	(0.0020)	27	3	3.17
Electron transfer flavoprotein β subunit, FixA	Rv3029c	28 kDa	(0.0020)	27	3	3.17
Fatty-acid-CoA ligase, FadD36	Rv1193	50 kDa	(0.0460)	9	1	3.17
Transferase	Rv1201c	33 kDa	(0.0460)	9	1	3.17
Phosphoribosylamine-glycine ligase, PurD	Rv0772	44 kDa	(0.0028)	26	3	3.12
Pyruvate kinase, PykA	Rv1617	51 kDa	(0.0021)	31	4	2.95
Low molecular weight protein antigen ,Cfp2	Rv2376c	17 kDa	(0.0250)	15	2	2.91
Glutamyl-tRNA	Rv3009c	55 kDa	(0.0000)	83	12	2.79
Transmembrane serine/threonine-protein kinase H, PknH	Rv1266c	67 kDa	(0.0036)	33	5	2.72
Conserved alanine-rich protein	Rv2744c	29 kDa	(0.0480)	13	2	2.70
Transmembrane serine/threonine-protein kinase D, PknD	Rv0931c	70 kDa	(0.0005)	51	8	2.67
Conserved hypothetical protein	Rv2159c	36 kDa	(0.0320)	18	3	2.58
ATP-dependent protease ATP-binding subunit, ClpC1	Rv3596c	94 kDa	(0.0000)	181	32	2.50
Glutamine synthetase, GlnA2	Rv2222c	50 kDa	(0.0280)	22	4	2.46
30 S ribosomal protein S1, RpsA	Rv1630	53 kDa	(0.0360)	21	4	2.39
Succinyl-CoA synthetase β chain, SucC	Rv0951	41 kDa	(0.0170)	40	9	2.15
Endopeptidase ATP-binding protein chain B, ClpB	Rv0384c	93 kDa	(0.0003)	131	33	1.99
Glutamine synthetase, GlnA1	Rv2220	54 kDa	(0.0200)	65	18	1.85
10-kDa chaperonin, GroES	Rv3418c	11 kDa	(0.0049)	136	41	1.73

[a] A value of 1 indicates an NSAF of 0.

of growth conditions (with more proteins available for comparison when profiled under normal growth). However, a few exceptions exist and are noteworthy. Specifically, Rv0350 (DnaK), Rv0384 (ClpB), and Rv3285 (AccA3) are found in both samples, but they demonstrate a reduced capacity to bind the ATP probe only under hypoxic growth conditions. Similarly, Rv0931 (PknD), Rv2780 (ald), and Rv3596 (ClpC1), are found in both samples, but they demonstrate a reduced capacity to bind the ATP probe only under normal growth conditions. This may be reflective of dynamic binding constants for ATP, based on the availability/loss of co-factors during different growth states. Several attractive drug targets were also identified in this analysis based on their increased abundance during hypoxic growth and their sensitivity to binding the ATP probe in the presence of excess ATPγS. Specifically, Rv0475 (Hbha), Rv0824 (DesA1), Rv0860 (FadB), Rv1297 (Rho), and Rv2477 represent this phenotype. Of these, Rv2477 is particularly attractive, as it is a macrolide ABC transporter and is associated with increased fluoroquinolone resistance (39). Other proteins, such as Rv0733 (Adk), Rv1310 (AtpD), and Rv3410 (GuaB3), are attractive targets based on the capacity to inhibit their binding and presence in *M. tuberculosis* regardless of growth state.

ATP-binding Proteins and Associated Biochemical Pathways—To find clusters of protein families functionally linked in relevant biochemical pathways, we utilized the list of 81 con-

TABLE II
Proteins with increased abundance during hypoxic growth

Identified proteins	Accession no.	Molecular mass	Fisher's exact test (*p* value)	Normal NSA[a]	Hypoxic NSAF	Log fold change
Conserved hypothetical protein	Rv2623	32 kDa	(0.0000)	1	14	−3.81
Acyl-(acyl-carrier protein) desaturase, DesA1	Rv0824c	39 kDa	(0.0000)	1	12	−3.58
Hypothetical protein, Acg	Rv2032	37 kDa	(0.0003)	1	8	−3.00
Phosphoribosylaminoimidazole-succinocarboxamide synthase, PurC	Rv0780	33 kDa	(0.0010)	1	7	−2.81
Ketol-acid reductoisomerase, IlvC	Rv3001c	36 kDa	(0.0010)	1	7	−2.81
Acyl-(acyl-carrier protein) desaturase DesA2	Rv1094	31 kDa	(0.0000)	2	12	−2.58
Isocitrate lyase, Icl	Rv0467	47 kDa	(0.0033)	1	6	−2.58
10-kDa culture filtrate antigen, EsxB	Rv3874	11 kDa	(0.0100)	1	5	−2.32
40-kDa secreted L-alanine dehydrogenase, Ald	Rv2780	39 kDa	(0.0000)	29	134	−2.21
Citrate synthase I, GltA2	Rv0896	48 kDa	(0.0320)	1	4	−2.00
DNA gyrase subunit B, GyrB	Rv0005	78 kDa	(0.0320)	1	4	−2.00
Transcription termination factor ρ	Rv1297	65 kDa	(0.0000)	4	15	−1.91
Iron-regulated heparin-binding hemagglutinin, HbhA	Rv0475	22 kDa	(0.0004)	3	11	−1.87
ATP synthase α chain, AtpA	Rv1308	59 kDa	(0.0011)	4	11	−1.46
Macrolide-transport ATP-binding protein ABC transporter	Rv2477c	62 kDa	(0.0005)	5	13	−1.38
6-Phosphofructokinase, PfkA	Rv3010c	37 kDa	(0.0140)	5	9	-0.85
Fatty-acid oxidation protein, FadB	Rv0860	76 kDa	(0.0010)	10	17	−0.77
Heat shock protein, HspX	Rv2031c	16 kDa	(0.0000)	133	223	−0.75
Conserved hypothetical protein	Rv1738	11 kDa	(0.0019)	10	16	−0.68
Bifunctional polyribonucleotide nucleotidyltransferase, GpsI	Rv2783c	80 kDa	(0.0026)	13	18	−0.47
Adenosylhomocysteinase, SahH	Rv3248c	54 kDa	(0.0000)	45	53	−0.24
Iron-regulated aconitate hydratase, Acn	Rv1475c	102 kDa	(0.0490)	10	11	−0.14

[a] A value of 1 indicates an NSAF of 0.

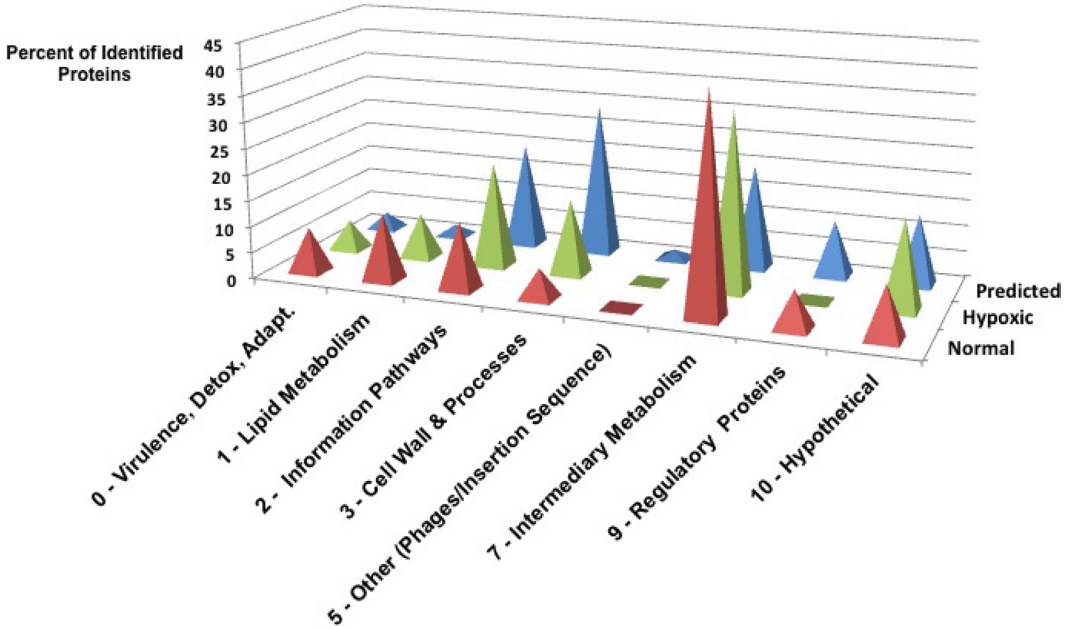

FIG. 4. **Comparison of functional categories.** Desthiobiotin-labeled proteins found to be differentially abundant between normal and hypoxic growth were sorted based on functional category and compared with proteins in each category predicted to be ATP binding. Categories 4 (Stable RNAs), 5 (Insertion Sequences and Phages), and 6 (PE/PPE) were not represented in the experimental ATPome dataset.

fidently labeled proteins and expanded our dataset to include nonlabeled proteins that were confidently identified by mass spectrometry (*i.e.* proteins with total spectral counts across biological replicates >5 with 90% peptide probability) irrespective of ATP labeling (supplemental Table S1). Functional association networks using the web-based Search Tool for

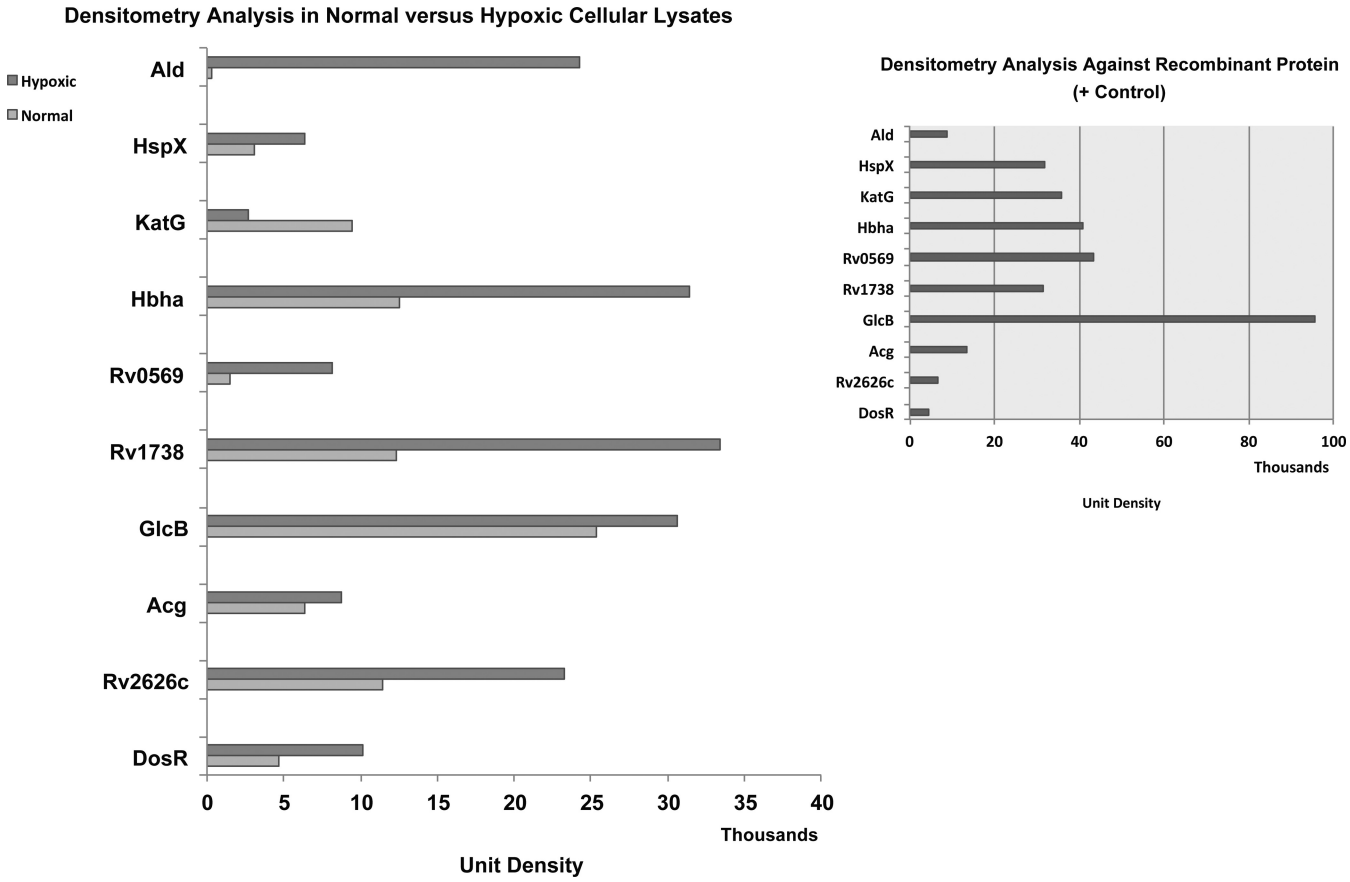

FIG. 5. **Densitometry analysis.** Several proteins found to be differentially abundant by NSAF were probed for immunoreactivity via Western blot. The densitometry analysis of these blots corroborates the differences in protein levels between Normal and Hypoxic growth (*left*). The densitometry of each protein with its corresponding positive control (recombinant protein) is reported (*upper*). All immunoblot images are provided in supplemental Fig. S1.

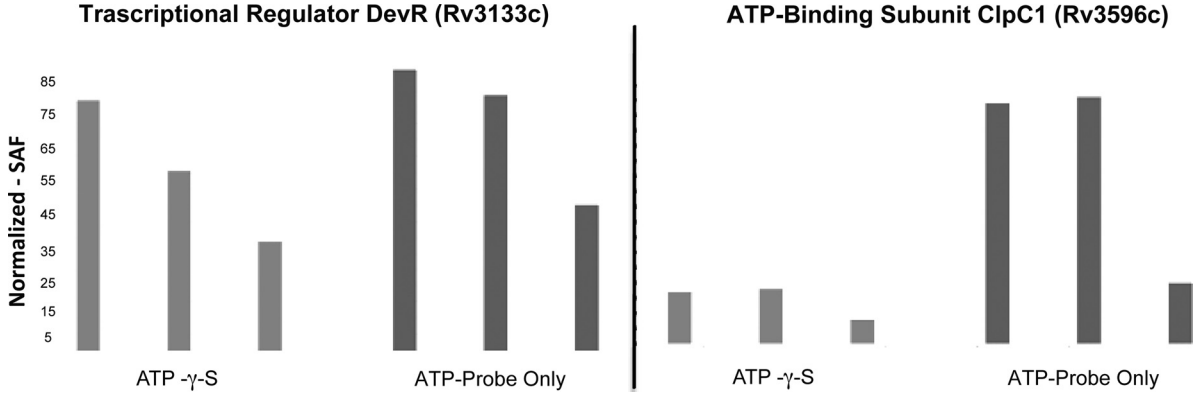

FIG. 6. **NSAF profiles of ATP-labeled peptides in the presence/absence of excess ATPγS.** Transient binding of ATP was observed in many proteins, including the DNA-binding transcriptional regulator DevR (*left*). In the presence of excess ATP (ATPγS), the spectral count profiles of the ATP-binding subunit of ClpC1 were significantly reduced (*right*) in cultures grown under normal conditions.

the Retrieval of Interacting Genes (STRING version 9.0) (22) were generated from the 81 ATP-binding proteins combined with the 54 unlabeled proteins. Emerging from this data set we visualized clusters of associated protein families (Fig. 7), including members of the polyketide synthase family (Category 1, Lipid Metabolism), ribosomal protein synthesis (Category 2, Information Pathways), and mycolic acid and peptidoglycan synthesis (Category 3, Cell Wall and Processes). Polyketide synthases are large multidomain proteins involved in lipid and mycolic acid biosynthesis. Pks5, Pks12, and Pks13 as well as the phthiocerol dimycoserate synthases PpsABCDE and mycocerosic acid synthase (Mas) work in

TABLE III
Competitive and transient binders of desthiobiotin-ATP in hypoxic cultures

	Gene no.	Molecular mass	*p* value	Avg. NSAF_ATPγS[a]	Avg. NSAF_ATP[b]	-Fold change
Competitive binders of desthiobiotin-ATP						
Fatty-acid oxidation protein, FadB	Rv0860	76 kDa	(0.0039)	1	6.33	6.33
Inosine-5-monophosphate dehydrogenase, GuaB3	Rv3410c	39 kDa	(0.0056)	1	6.00	6.00
Transcription termination factor ρ	Rv1297	65 kDa	(0.0079)	1	5.67	5.67
Macrolide-transport ATP-binding protein, ABC transporter	Rv2477c	62 kDa	(0.0160)	1	5.00	5.00
Endopeptidase ATP-binding protein chain B, ClpB	Rv0384c	93 kDa	(0.0031)	2.5	11.67	4.67
Iron-regulated heparin-binding hemagglutinin, HbhA	Rv0475	22 kDa	(0.0320)	1	4.33	4.33
Adenosylhomocysteinase, SahH	Rv3248c	54 kDa	(0.0065)	5.5	18.33	3.33
Chaperone protein, DnaK	Rv0350	67 kDa	(0.0001)	16	50.00	3.13
Adenylate kinase, Adk	Rv0733	20 kDa	(0.0400)	8	20.33	2.54
Acyl-(acyl-carrier protein) desaturase, DesA1[c]	Rv0824c	39 kDa	(0.2200)	2	4.67	2.33
ATP synthase β chain, AtpD[c]	Rv1310	53 kDa	(0.1500)	5	11.33	2.27
Bifunctional acetyl-/propionyl-coenzyme A carboxylase α chain, AccA3[c]	Rv3285	64 kDa	(0.2600)	3	6.33	2.11
Transient binders of desthiobiotn-ATP						
50 S ribosomal protein L7/L12, RplL	Rv0652	13 kDa	(0.3100)	4.5	8.67	1.93
10-kDa chaperonin, GroES	Rv3418c	11 kDa	(0.3600)	8	14.33	1.79
ATP-dependent protease ATP-binding subunit, ClpC1	Rv3596c	94 kDa	(0.5000)	7	11.33	1.62
60-kDa chaperonin 1, GroEL1	Rv3417c	56 kDa	(0.5100)	3.5	5.67	1.62
Conserved hypothetical protein	Rv2623	32 kDa	(0.5600)	3.5	5.33	1.52
40-kDa secreted L-alanine dehydrogenase, Ald	Rv2780	39 kDa	(0.0520)	36	45.33	1.26
Cold shock protein A, CspA	Rv3648c	7 kDa	(0.4400)	4	5.00	1.25
60-kDa chaperonin 2, GroEL2	Rv0440	57 kDa	(0.0000)	135	168.67	1.25
Heat shock protein, HspX	Rv2031c	16 kDa	(0.0002)	67.5	75.00	1.11
Transmembrane serine/threonine-protein kinase A, PknA	Rv0015c	46 kDa	(0.3100)	4	4.33	1.08
Isocitrate lyase, Icl	Rv0467	47 kDa	(0.4300)	2.5	2.67	1.07
Integration host factor, MihF	Rv1388	21 kDa	(0.0280)	19	20.00	1.05
6-Phosphofructokinase, PfkA	Rv3010c	37 kDa	(0.3200)	3.5	3.67	1.05
Bifunctional polyribonucleotide nucleotidyltransferase, GpsI	Rv2783c	80 kDa	(0.1600)	6.5	6.67	1.03
Iron-regulated elongation factor tu tuf	Rv0685	44 kDa	(0.0120)	20.5	20.33	0.99
Propionyl-CoA carboxylase β chain 5, AccD5	Rv3280	59 kDa	(0.5000)	1.5	1.33	0.89
Conserved hypothetical protein	Rv3269	10 kDa	(0.1600)	4.5	4.00	0.89
Electron transfer flavoprotein β subunit, FixA	Rv3029c	28 kDa	(0.3300)	2	1.67	0.83
Conserved hypothetical protein	Rv1738	11 kDa	(0.0390)	7.5	6.00	0.80
Iron-regulated conserved hypothetical protein	Rv1636	15 kDa	(0.0093)	10	7.33	0.73
Transmembrane serine/threonine-protein kinase D, PknD	Rv0931c	70 kDa	(0.0100)	6	3.33	0.56
Conserved hypothetical protein	Rv3127	39 kDa	(0.0640)	3	1.67	0.56

[a] Average spectral count of desthiobiotin-labeled peptides in the presence of 500 μM ATPγS. A value of 1 indicates 0 spectral counts in the presence of excess ATP analog.
[b] Average spectral count of desthiobiotin-labeled peptides with no excess ATPγS.
[c] *p* value of >0.05.

coordination to synthesize the cell wall-associated and virulence determinant phthiocerol dimycocerosate (40, 41). Within this group of proteins, PpsC was found to bind ATP. PpsC catalyzes the complete reduction of malonyl-CoA in the synthesis of phthiocerol. The localization of the ATP nucleotide probe was not within any of the annotated domains of PpsC.

TABLE IV
Competitive and transient binders of desthiobiotin-ATP in normal cultures

	Gene no.	Molecular mass	*p* value	Avg. NSAF_ATPγS[a]	Avg. NSAF_ATP[b]	Fold change
Competitive Binders of Desthiobiotin-ATP						
Acetyl-/propionyl-CoA carboxylase α subunit, AccA1	Rv2501c	71 kDa	(0.0000)	1.00	15.67	15.67
Glutamyl-tRNA amidotransferase subunit B, GatB	Rv3009c	55 kDa	(0.0000)	2.33	28.33	12.14
Inosine-5-monophosphate dehydrogenase, GuaB3	Rv3410c	39 kDa	(0.0000)	1.00	11.67	11.67
Transmembrane serine/threonine-protein kinase H, PknH	Rv1266c	67 kDa	(0.0000)	1.00	11.33	11.33
Fatty-acid-CoA ligase, FadD7	Rv0119	55 kDa	(0.0000)	1.00	9.67	9.67
Phosphoribosylamine-glycine ligase, PurD	Rv0772	44 kDa	(0.0000)	1.00	9.33	9.33
Tryptophanyl-tRNA synthetase, TrpS	Rv3336c	36 kDa	(0.0001)	1.00	7.00	7.00
Polyphosphate kinase, Ppk	Rv2984	83 kDa	(0.0000)	3.33	22.67	6.80
Phosphoglycerate kinase, Pgk	Rv1437	43 kDa	(0.0000)	3.00	19.67	6.56
Cysteinyl-tRNA synthetase 1, CysS1	Rv3580c	52 kDa	(0.0005)	1.00	5.67	5.67
Fatty-acid-CoA ligase, FadD23	Rv3826	63 kDa	(0.0014)	1.00	5.00	5.00
Universal stress protein	Rv2319c	32 kDa	(0.0012)	1.33	6.33	4.75
CTP synthase, PyrG	Rv1699	64 kDa	(0.0024)	1.00	4.67	4.67
Phosphofructokinase, PfkB	Rv2029c	35 kDa	(0.0073)	1.00	4.00	4.00
ATP-dependent protease ATP-binding subunit, ClpC1	Rv3596c	94 kDa	(0.0000)	15.33	61.00	3.98
Anchored-membrane serine/threonine-protein kinase, PknF	Rv1746	51 kDa	(0.0130)	1.00	3.67	3.67
Chaperone protein, HtpG	Rv2299c	73 kDa	(0.0130)	1.00	3.67	3.67
DNA polymerase I, PolA	Rv1629	98 kDa	(0.0078)	1.67	6.00	3.60
Acetate kinase, AckA	Rv0409	41 kDa	(0.0220)	1.00	3.33	3.33
UDP-*N*-acetylmuramoylalanyl-D-glutamyl-2,6-diaminopimelate-D-alanyl-D-alanyl ligase, MurF	Rv2157c	52 kDa	(0.0220)	1.00	3.33	3.33
Conserved hypothetical protein	Rv3282	23 kDa	(0.0220)	1.00	3.33	3.33
Conserved hypothetical protein	Rv2510c	57 kDa	(0.0220)	1.00	3.33	3.33
Fatty-acid-CoA ligase, FadD28	Rv2941	63 kDa	(0.0077)	2.33	7.67	3.29
Nucleoside diphosphate kinase, NdkA	Rv2445c	15 kDa	(0.0150)	2.00	6.33	3.17
40-kDa secreted L-alanine dehydrogenase, Ald	Rv2780	39 kDa	(0.0066)	3.00	9.33	3.11
Adenosylhomocysteinase, SahH	Rv3248c	54 kDa	(0.0017)	5.00	15.00	3.00
Pyruvate kinase, PykA	Rv1617	51 kDa	(0.0053)	3.67	11.00	3.00
Malate synthase G, GlcB	Rv1837c	80 kDa	(0.0420)	1.67	4.67	2.80
Aldehyde dehydrogenase	Rv0458	55 kDa	(0.0350)	2.67	7.00	2.63
Adenylate kinase, Adk	Rv0733	20 kDa	(0.0035)	17.33	36.67	2.12
transmembrane serine/threonine-protein kinase D, PknD	Rv0931c	70 kDa	(0.0400)	8.67	17.67	2.04
ATP synthase β chain, AtpD	Rv1310	53 kDa	(0.0250)	13.33	26.33	1.98
Transient binders of desthiobiotin-ATP						
Endopeptidase ATP-binding protein chain B, ClpB	Rv0384c	93 kDa	(0.0410)	25.33	44.33	1.75
3-Hydroxyacyl-thioester dehydrogenase, HtdY	Rv3389c	30 kDa	(0.4000)	4.67	7.00	1.50
Iron-regulated short-chain dehydrogenase/reductase	Rv3224	30 kDa	(0.4100)	6.33	9.33	1.47
Aminomethyltransferase, GcvT	Rv2211c	40 kDa	(0.4300)	4.33	6.33	1.46
Phosphopantetheine adenylyltransferase, KdtB	Rv2965c	18 kDa	(0.4700)	2.33	3.33	1.43
Chaperone protein, DnaK	Rv0350	67 kDa	(0.3800)	40.00	57.00	1.43
Cold shock protein A, CspA	Rv3648c	7 kDa	(0.5300)	5.67	7.67	1.35
Secreted fibronectin-binding protein antigen	85-B fbpB	Rv1886c	35 kDa	(0.5400)	2.00	2.67
Iron-regulated peptidyl-prolyl *cis-trans* isomerase, PpiA	Rv0009	19 kDa	(0.5400)	3.00	4.00	1.33
Glutamine synthetase, GlnA2	Rv2222c	50 kDa	(0.5500)	6.00	8.00	1.33
Pyruvate dehydrogenase E2 component, SucB	Rv2215	57 kDa	(0.5500)	7.33	9.67	1.32
Acyl-CoA dehydrogenase, FadE5	Rv0244c	66 kDa	(0.5700)	3.33	4.33	1.30
Pyruvate dehydrogenase E1 component, AceE	Rv2241	100 kDa	(0.5700)	4.67	6.00	1.29
60-kDa chaperonin 2, GroEL2	Rv0440	57 kDa	(0.0180)	279.00	352.00	1.26
Iron-regulated conserved hypothetical protein	Rv1636	15 kDa	(0.3500)	17.00	21.00	1.24
Propionyl-CoA carboxylase β chain 5, AccD5	Rv3280	59 kDa	(0.5800)	3.00	3.67	1.22
Low molecular weight protein antigen, Cfp2	Rv2376c	17 kDa	(0.5000)	4.67	5.67	1.21
Glutamine synthetase, GlnA1	Rv2220	54 kDa	(0.3000)	17.67	21.33	1.21
Heat shock protein, HspX	Rv2031c	16 kDa	(0.1800)	36.00	43.33	1.20

Table IV —*continued*

	Gene no.	Molecular mass	*p* value	Avg. NSAF_ATPγS[a]	Avg. NSAF_ATP[b]	Fold change
Succinyl-CoA synthetase β chain, SucC	Rv0951	41 kDa	(0.3500)	11.67	14.00	1.20
Oligoribonuclease, Orn	Rv2511	23 kDa	(0.4800)	5.00	6.00	1.20
Protein transport protei, SecE2	Rv0379	8 kDa	(0.5400)	3.33	4.00	1.20
L-Lactate dehydrogenase, LldD2	Rv1872c	45 kDa	(0.4500)	5.33	6.33	1.19
Conserved hypothetical protein	Rv2159c	36 kDa	(0.4300)	5.67	6.67	1.18
Bifunctional coenzyme A carboxylase α chain, AccA3	Rv3285	64 kDa	(0.2800)	13.67	16.00	1.17
50 S ribosomal protein L7/L12, RplL	Rv0652	13 kDa	(0.2500)	16.00	18.67	1.17
Conserved hypothetical protein	Rv3269	10 kDa	(0.4800)	4.00	4.67	1.17
Ribosome recycling factor, Frr	Rv2882c	21 kDa	(0.5700)	2.33	2.67	1.14
Superoxide dismutase, SodA	Rv3846	23 kDa	(0.3900)	5.33	6.00	1.13
Transmembrane serine/threonine-protein kinase E, PknE	Rv1743	61 kDa	(0.3900)	5.33	6.00	1.13
Two-component system transcriptional regulator, DevR	Rv3133c	23 kDa	(0.4600)	3.33	3.67	1.10
Tetrahydrodipicolinate *N*-succinyltransferase	Rv1201c	33 kDa	(0.4600)	3.33	3.67	1.10
Leucyl-tRNA synthetase, LeuS	Rv0041	108 kDa	(0.3800)	4.33	4.67	1.08
Iron-regulated elongation factor tu tuf	Rv0685	44 kDa	(0.0300)	40.33	43.33	1.07
Immunogenic protein, Mpt64	Rv1980c	25 kDa	(0.3000)	6.00	6.33	1.06
30 S ribosomal protein S1, RpsA	Rv1630	53 kDa	(0.2500)	7.33	7.67	1.05
Transmembrane serine/threonine-protein kinase A, PknA	Rv0015c	46 kDa	(0.2100)	8.67	9.00	1.04
Transcriptional regulator	Rv0023	27 kDa	(0.5600)	1.67	1.67	1.00
Hypothetical protein, Wag31	Rv2145c	28 kDa	(0.4200)	2.67	2.67	1.00
Hypothetical protein	Rv3818	58 kDa	(0.5000)	2.00	2.00	1.00
Conserved alanine-rich protein	Rv2744c	29 kDa	(0.2800)	5.00	5.00	1.00
Enoyl-CoA hydratase, EchA9	Rv1071c	36 kDa	(0.3900)	3.00	3.00	1.00
Conserved hypothetical protein	Rv2140c	19 kDa	(0.5000)	2.00	2.00	1.00
Thiosulfate sulfurtransferase, CysA2	Rv0815c	31 kDa	(0.5600)	1.67	1.67	1.00
Zinc-type alcohol dehydrogenase NAD-dependent, AdhB	Rv0761c	40 kDa	(0.2300)	4.67	4.33	0.93
Transcriptional regulator, MoxR1	Rv1479	41 kDa	(0.2800)	3.33	3.00	0.90
60-kDa chaperonin 1, GroEL1	Rv3417c	56 kDa	(0.0270)	16.33	14.67	0.90
Meromycolate extension acyl carrier protein, AcpM	Rv2244	13 kDa	(0.1400)	6.33	5.67	0.89
Haloalkane dehalogenase	Rv2296	33 kDa	(0.1500)	6.00	5.33	0.89
Succinyl-CoA synthetase α chain, SucD	Rv0952	31 kDa	(0.1600)	5.67	5.00	0.88
ATP synthase α chain, AtpA	Rv1308	59 kDa	(0.3300)	2.33	2.00	0.86
Integration host factor, MihF	Rv1388	21 kDa	(0.0001)	41.33	34.67	0.84
acyl-CoA dehydrogenase, FadE25	Rv3274c	42 kDa	(0.3500)	2.00	1.67	0.83
DNA polymerase III β chain, DnaN	Rv0002	42 kDa	(0.3500)	2.00	1.67	
Pyridoxamine 5-phosphate oxidase, PdxH	Rv2607	25 kDa	(0.1100)	5.67	4.67	0.82
10-kDa chaperonin, GroES	Rv3418c	11 kDa	(0.0000)	50.33	40.67	0.81
Iron-regulated aconitate hydratase, Acn	Rv1475c	102 kDa	(0.1200)	5.00	4.00	0.80
30 S ribosomal protein S16, RpsP	Rv2909c	17 kDa	(0.3800)	1.67	1.33	0.80
Hypothetical protein, Cfp17	Rv1827	17 kDa	(0.2000)	3.33	2.67	0.80
Fructose-bisphosphate aldolase, Fba	Rv0363c	37 kDa	(0.2000)	3.00	2.33	0.78
Short-chain type dehydrogenase/reductase	Rv0148	30 kDa	(0.2000)	3.00	2.33	0.78
Transcriptional regulator, TetR family	Rv0144	31 kDa	(0.2000)	3.00	2.33	0.78
19-kDa lipoprotein antigen precursor, LpqH	Rv3763	15 kDa	(0.0250)	8.67	6.33	0.73
Conserved hypothetical protein	Rv2406c	15 kDa	(0.2100)	2.33	1.67	0.71
Electron transfer flavoprotein β subunit, FixA	Rv3029c	28 kDa	(0.0039)	13.67	9.67	0.71
Enolase, Eno	Rv1023	45 kDa	(0.1300)	3.33	2.33	0.70

[a] Average spectral count of desthiobiotin-labeled peptides was in the presence of 500 μM ATPγS. A value of 1 indicates 0 spectral counts in the presence of excess ATP analog.

[b] Average spectral count of desthiobiotin-labeled peptides with no excess ATPγS.

Although PpsC is a nonessential enzyme, its associated protein partners identified in this study do play essential roles (pks12/13) (41).

A known target for the antimycobacterial drug rifampin (RpoB) and other peripheral ribosomal proteins was distinctly represented in our interaction data set (Fig. 7); however, none

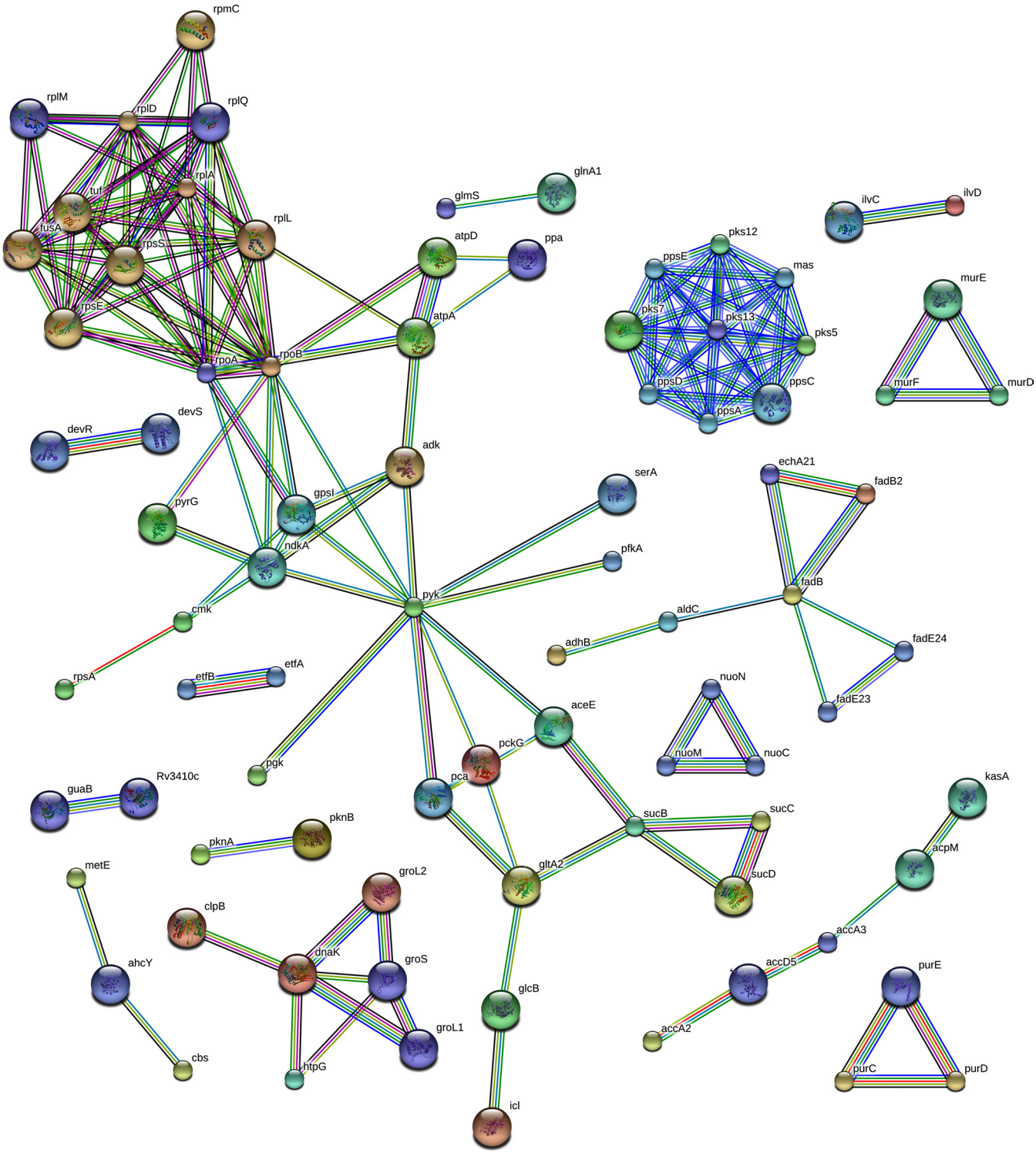

FIG. 7. **Protein-protein interaction networks of the *M. tuberculosis* ATPome.** The list of protein IDs from our MS analysis was input into the STRING database (STRING version 9.0) to identify known and predicted functional networks. 48% of the proteins in our shotgun analysis were shown to be functionally associated with at least one known interacting partner. Emerging protein clusters are functionally relevant in basic metabolism (*i.e.* respiratory chain and protein synthesis), cell wall biosynthesis (*i.e.* fatty acid and peptidoglycan synthesis), and virulence (*i.e.* lipid synthesis).

were found to be differentially abundant between normal and hypoxic states. We identified 16 gene products involved in the synthesis of proteins, 14 of which are essential.

Proteins involved in fatty acid and mycolic acid biosynthesis found within our mycobacterial ATPome are listed in supplemental Table S1. Of note, the essential acyl (ACP) membrane-bound desaturases, DesA1 and DesA2, catalyze the introduction of the first double bond in saturated C16 and C18 fatty acids. *desA1* and *desA2* are essential genes for mycobacterial survival, and DesA1 is predicted to be a relevant drug target based on interactome and genome-scale structural analysis (42). Both enzymes were found to be in higher abundance during hypoxia with a log FC of 12 and 6, respectively (Table I). A third member of this family DesA3 is a putative target of the thiourea drug isoxyl (43), but it was not identified in our study. The *M. tuberculosis* genome contains three biotin-dependent essential acyl-CoA carboxylases (AccA1–3). Although the biotin binding domain of these enzymes did allow for the nonspecific attachment to the streptavidin capture affinity resin (as discussed above), their ATP-binding function is essential to their enzymatic activity, and labeling with nucleotide probe was located within an annotated nucleotide binding domain (Lys-116) (44).

Finally, we identified the D-glutamic acid ligase (MurD), the *meso*-diaminopimelic acid ligase (MurE), and the dipeptide D-Ala-D-Ala ligase (MurF) in our ATPome dataset. Interestingly, we also identified the dihyrodipicolinate reductase (DapB). Although primarily associated with processes of intermediary metabolism due to its function in the biosynthesis of L-lysine, it is also involved in the synthesis of *meso*-diaminopimelic acid, an amino acid contained in the core tetrapeptide of peptidoglycan (45). An *M. tuberculosis* mutant lacking functional DapB has been classified as a slow growth mutant (46), and this protein may represent a uniquely lethal drug target as this metabolic function is unique to prokaryotes.

DISCUSSION

The results represented in this study are among the first to describe the ATP-binding proteome of the pathogenic organism, *M. tuberculosis* and present a relevant proteomic comparison between normally growing and hypoxic state bacteria. The majority of these proteins are essential gene products and may be relevant therapeutic targets. We quantitatively measured the differences in protein levels between normally growing and hypoxic state bacteria and provided preliminary data into the binding characteristics and utilization of ATP across multiple classes of functional enzymes. Using desthiobiotin nucleotide probes in competition with ATP analogs provides the framework necessary to pursue antimicrobial inhibitors whose mode of action relies on competition within the ATP-binding site of select protein targets (4, 47). The utilization of ATP in lipid and cell wall biosynthesis pathways makes it tempting to speculate that a selective and broad-spectrum nucleotide-competitive compound may affect these critical processes in such a way as to alter cell wall architecture and integrity. Because the cell wall of *M. tuberculosis* is a potent barrier against small molecule therapeutics, agents that alter the cell wall have been shown to increase drug sensitivity and help circumvent the problems of multidrug and extensively drug-resistant bacteria (48).

Beyond the identification of these proteins as targets for small molecule inhibitors, the ATP-binding proteins of *M. tuberculosis* comprise a very unique and functional subset of the *M. tuberculosis* proteome. The distribution of ATP-binding proteins among a variety of functional classes supports the general hypothesis that proteins of the mycobacterial ATPome provide necessary mechanisms of adaptation utilized in the maintenance of growth under a variety of microenvironmental conditions. Applying functional categories across a predicted subset of ATP-binding proteins demonstrated several features of note: 1) The predicted ATP-binding protein distribution by function more closely reflects experimentally identified proteins grown under normal conditions, 2) Lipid biosynthesis and intermediary metabolism are overly represented experimentally, and compared with predicted annotations, a trend recently seen elsewhere (26), 3) Predictions for cell wall and processes were under-represented experimentally compared with predicted subsets. This is most likely due to our experimental approaches, and further investigation of the ATP-binding properties of cell wall proteins may lead to better experimental representation within this category. The functional Category 10, Conserved Hypotheticals, represents proteins whose function remains uncharacterized and accounts for approximately one-quarter of the *M. tuberculosis* proteome. Recent re-annotation and prediction efforts concluded that the majority of hypothetical proteins could be redistributed among the categories of Small Molecule Metabolism, Cell Wall Processes, and Lipid Metabolism (49, 50). The utilization of ATP by these hypothetical proteins may provide further insight into their cellular roles and enzymatic functions and further lead to key insights in the study of *M. tuberculosis* pathogenicity. The idea of ATP binding and hydrolysis acting as a molecular switch controlling the transition into hypoxia has been observed in the study of mammalian models of low-oxygen conditions (51, 52). For mycobacteria, one class of ATP-binding proteins, the Universal Stress Proteins (USPs), may be involved in the responses to changes in environmental and nutrient conditions leading to variations in virulence and adaptation. The USPs identified in our study include Rv2005c, Rv2028c, Rv2319c, Rv2623, Rv2624, and Rv2626c. Several years ago, Drumm and Chan *et al.* (53), investigated the nucleotide binding capabilities of Rv2623 and its role as an USP. Gene deletion mutants in *M. tuberculosis* demonstrated a hypervirulent phenotype that failed to enter into dormancy within susceptible Hartley guinea pigs. Disruption of the ATP-binding site of Rv2623 resulted in similar attenuated phenotypes described for the deletion mutants. It was hypothesized that the binding of ATP by similar USPs could be a regulatory

mechanism utilized in the transition from normal growth to an oxygen-poor state of dormancy.

In our profile of ATP-binding proteins from normally and hypoxically grown *M. tuberculosis*, we identified several proteins known to be under the control of the dormancy regulon *dosR*. The DevR-DevS two component system (TCS) is implicated in virulence and mediates the expression of ~48 dormancy-associated genes when *M. tuberculosis* adapts to hypoxia and is exposed to other stress factors like nitric oxide, carbon monoxide, and ascorbic acid (54). The ~48 genes that comprise the *devR* dormancy regulon include well known genes like *hspX* (the α-crystallin like chaperone), the nitrate reductase *acg,* and several uncharacterized hypothetical proteins such as Rv0569, Rv1738, and Rv2626c. A derivative of phenylcoumarin reduced the survival of hypoxically adapted *M. tuberculosis* and also inhibited DevR binding to target DNA (55). We would expect to have identified the sensor kinase DevS; however, it did not meet criteria for final inclusion, most likely due to its subcellular location with the plasma membrane. The response regulator DevR/DosR (Rv3133c) was shown to be confidently labeled with the ATP probe at the C-terminal DNA binding domain. In our competition experiments with 100-fold excess ATPγS, the desthiobiotin nucleotide probe was still able to bind and label two lysines (Lys-179 and Lys-182) within the helix-turn-helix DNA binding domain of DevR (UniProt ID >sp|P951931|167–186). The physiological implications of nucleotide binding to DevR remain to be elucidated, although Ansong *et al.* (26), also observed this phenomena for DNA-binding proteins. Genomic scale surveys of essential genes of *M. tuberculosis* and transcriptome-wide analyses of the bacterial response to environmental or metabolic conditions mimicking the host environment have been carried out in the pursuit of attractive, novel, and functionally relevant drug targets (30, 56, 57). Additionally, large scale proteomic profiling under simulated *in vitro* conditions or *in vivo* have also been performed (58–60). However, models of gene regulation, protein-protein interactions, and unique metabolic pathways at the systems level remains incomplete, especially those designed to characterize functional changes that mediate the switch into dormancy and thus may be key therapeutic targets for latent tuberculosis (61, 62). Through the study of the *M. tuberculosis* ATPome, we have defined a functionally linked analysis among essential gene products of the mycobacterial proteome. Furthermore, the chemoproteomic technique employed in these studies may be used to broaden the functional annotations and physiological roles of many of these nucleotide-binding proteins, especially in response to differing metabolic conditions. For drug discovery efforts, this work supports a growing body of evidence regarding the potential of pursuing antimicrobial inhibitors whose mode of action relies on competition within the ATP-binding site of select proteins (5, 47, 63–65). Future studies focused on measuring the abundance levels of promising inhibitor targets throughout the course of infection in *M. tuberculosis*, as well as similar studies in other biologically important pathogens that persist in multiple growth and metabolic states, will further demonstrate the broad applicability of this technique in drug discovery programs.

Acknowledgments—We thank Phillip Knabenbauer for assistance with the growth and manipulation of *M. tuberculosis* and Tige Rustad at the Seattle Biomedical Research Institute for providing information regarding growth of *M. tuberculosis* under hypoxia.

* This work was supported, in whole or in part, by National Institutes of Health Grant HHSN266200400091c from NIAID (to K.M.D.). This work was also supported by administrative funds by the Colorado State University Department of Microbiology, Immunology, and Pathology (to K.M.D.).

S This article contains supplemental material.

The mass spectrometry proteomics data have been deposited to the ProteomeXchange Consortium (http://proteomecentral.proteomexchange.org) via the PRIDE partner repository (*16*) *with the dataset identifier PXD000141.*

[e] Recipient of a postdoctoral fellowship grant from Indo-US Science and Technology Forum.

[g] Supported by the Center for Computational Science of the University of Miami.

[j] To whom correspondence should be addressed. Tel.: 970-491-1891; Fax: 970-491-1815; E-mail: kdobos@colostate.edu.

REFERENCES

1. World Health Organization (2011) WHO Report 2011: Global Tuberculosis Control. World Health Organization, Geneva
2. Ananthan, S., Faaleolea, E. R., Goldman, R. C., Hobrath, J. V., Kwong, C. D., Laughon, B. E., Maddry, J. A., Mehta, A., Rasmussen, L., Reynolds, R. C., Secrist, J. A., 3rd, Shindo, N., Showe, D. N., Sosa, M. I., Suling, W. J., and White, E. L. (2009) High-throughput screening for inhibitors of *Mycobacterium tuberculosis* H37Rv. *Tuberculosis* **89,** 334–353
3. Magnet, S., Hartkoorn, R. C., Székely, R., Pató, J., Triccas, J. A., Schneider, P., Szántai-Kis, C., Orfi, L., Chambon, M., Banfi, D., Bueno, M., Turcatti, G., Kéri, G., and Cole, S. T. (2010) Leads for antitubercular compounds from kinase inhibitor library screens. *Tuberculosis* **90,** 354–360
4. Reynolds, R. C., Ananthan, S., Faaleolea, E., Hobrath, J. V., Kwong, C. D., Maddox, C., Rasmussen, L., Sosa, M. I., Thammasuvimol, E., White, E. L., Zhang, W., and Secrist, J. A., 3rd (2012) High throughput screening of a library based on kinase inhibitor scaffolds against *Mycobacterium tuberculosis* H37Rv. *Tuberculosis* **92,** 72–83
5. Triola, G., Wetzel, S., Ellinger, B., Koch, M. A., Hübel, K., Rauh, D., and Waldmann, H. (2009) ATP competitive inhibitors of D-alanine-D-alanine ligase based on protein kinase inhibitor scaffolds. *Bioorg. Med. Chem.* **17,** 1079–1087
6. Vetter, M. L., Rodgers, M. A., Patricelli, M. P., and Yang, P. L. (2012) *ACS Chem. Biol.* **7,** 2019–2026.
7. Sadler, N. C., Angel, T. E., Lewis, M. P., Pederson, L. M., Chauvigné-Hines, L. M., Wiedner, S. D., Zink, E. M., Smith, R. D., and Wright, A. T. (2012) Activity-based protein profiling reveals mitochondrial oxidative enzyme impairment and restoration in diet-induced obese mice. *PLoS One* **7,** e47996
8. Kumari, S., and Ram, V. J. (2004) Advances in molecular targets and chemotherapy of tuberculosis. *Drugs Today* **40,** 487–500
9. Patricelli, M. P., Nomanbhoy, T. K., Wu, J., Brown, H., Zhou, D., Zhang, J., Jagannathan, S., Aban, A., Okerberg, E., Herring, C., Nordin, B., Weissig, H., Yang, Q., Lee, J. D., Gray, N. S., and Kozarich, J. W. (2011) *In situ* kinase profiling reveals functionally relevant properties of native kinases. *Chem. Biol.* **18,** 699–710
10. Patricelli, M. P., Szardenings, A. K., Liyanage, M., Nomanbhoy, T. K., Wu, M., Weissig, H., Aban, A., Chun, D., Tanner, S., and Kozarich, J. W. (2007) Functional interrogation of the kinome using nucleotide acyl phosphates. *Biochemistry* **46,** 350–358
11. Bantscheff, M., Eberhard, D., Abraham, Y., Bastuck, S., Boesche, M.,

Hobson, S., Mathieson, T., Perrin, J., Raida, M., Rau, C., Reader, V., Sweetman, G., Bauer, A., Bouwmeester, T., Hopf, C., Kruse, U., Neubauer, G., Ramsden, N., Rick, J., Kuster, B., and Drewes, G. (2007) Quantitative chemical proteomics reveals mechanisms of action of clinical ABL kinase inhibitors. *Nat. Biotechnol.* **25,** 1035–1044

12. Li, J., Rix, U., Fang, B., Bai, Y., Edwards, A., Colinge, J., Bennett, K. L., Gao, J., Song, L., Eschrich, S., Superti-Furga, G., Koomen, J., and Haura, E. B. (2010) A chemical and phosphoproteomic characterization of dasatinib action in lung cancer. *Nat. Chem. Biol.* **6,** 291–299
13. Yang, H., Troudt, J., Grover, A., Arnett, K., Lucas, M., Cho, Y. S., Bielefeldt-Ohmann, H., Taylor, J., Izzo, A., and Dobos, K. M. (2011) Three protein cocktails mediate delayed-type hypersensitivity responses indistinguishable from that elicited by purified protein derivative in the guinea pig model of *Mycobacterium tuberculosis* infection. *Infect. Immun.* **79,** 716–723
14. Cho, Y. S., Dobos, K. M., Prenni, J., Yang, H., Hess, A., Rosenkrands, I., Andersen, P., Ryoo, S. W., Bai, G. H., Brennan, M. J., Izzo, A., Bielefeldt-Ohmann, H., and Belisle, J. T. (2012) Deciphering the proteome of the *in vivo* diagnostic reagent "purified protein derivative " from *Mycobacterium tuberculosis*. *Proteomics* **12,** 979–991
15. Eng, J. K., Searle, B. C., Clauser, K. R., and Tabb, D. L. (2011) A face in the crowd: recognizing peptides through database search. *Mol. Cell. Proteomics* **10,** R111.009522
16. Vizcaíno, J. A., Côté, R. G., Csordas, A., Dianes, J. A., Fabregat, A., Foster, J. M., Griss, J., Alpi, E., Birim, M., Contell, J., O'Kelly, G., Schoenegger, A., Ovelleiro, D., Pérez-Riverol, Y., Reisinger, F., Ríos, D., Wang, R., and Hermjakob, H. (2013) The PRoteomics IDEntifications (PRIDE) database and associated tools: status in 2013. *Nucleic Acids Res.* **41,** D1063–D1069
17. Li, M., Gray, W., Zhang, H., Chung, C. H., Billheimer, D., Yarbrough, W. G., Liebler, D. C., Shyr, Y., and Slebos, R. J. (2010) Comparative shotgun proteomics using spectral count data and quasi-likelihood modeling. *J. Proteome Res.* **9,** 4295–4305
18. Conesa, A., Götz, S., García-Gómez, J. M., Terol, J., Talón, M., and Robles, M. (2005) Blast2GO: a universal tool for annotation, visualization, and analysis in functional genomics research. *Bioinformatics* **21,** 3674–3676
19. Keller, A., Nesvizhskii, A. I., Kolker, E., and Aebersold, R. (2002) Empirical statistical model to estimate the accuracy of peptide identifications made by MS/MS and database search. *Anal. Chem.* **74,** 5383–5392
20. Fischer, G., and Schmid, F. X. (1990) The mechanism of protein folding. Implications of *in vitro* refolding models for *de novo* protein folding and translocation in the cell. *Biochemistry* **29,** 2205–2212
21. Norman, E., De Smet, K. A., Stoker, N. G., Ratledge, C., Wheeler, P. R., and Dale, J. W. (1994) Lipid synthesis in mycobacteria: characterization of the biotin carboxyl carrier protein genes from *Mycobacterium leprae* and *M. tuberculosis*. *J. Bacteriol.* **176,** 2525–2531
22. Szklarczyk, D., Franceschini, A., Kuhn, M., Simonovic, M., Roth, A., Minguez, P., Doerks, T., Stark, M., Muller, J., Bork, P., Jensen, L. J., and von Mering, C. (2011) The STRING database in 2011: functional interaction networks of proteins, globally integrated and scored. *Nucleic Acids Res.* **39,** D561–D568
23. Griffin, J. E., Gawronski, J. D., Dejesus, M. A., Ioerger, T. R., Akerley, B. J., and Sassetti, C. M. (2011) High-resolution phenotypic profiling defines genes essential for mycobacterial growth and cholesterol catabolism. *PLoS Pathog.* **7,** e1002251
24. Sassetti, C. M., Boyd, D. H., and Rubin, E. J. (2003) Genes required for mycobacterial growth defined by high density mutagenesis. *Mol. Microbiol.* **48,** 77–84
25. Punta, M., Coggill, P. C., Eberhardt, R. Y., Mistry, J., Tate, J., Boursnell, C., Pang, N., Forslund, K., Ceric, G., Clements, J., Heger, A., Holm, L., Sonnhammer, E. L., Eddy, S. R., Bateman, A., and Finn, R. D. (2012) The Pfam protein families database. *Nucleic Acids Res.* **40,** D290–D301
26. Ansong, C., Ortega, C., Payne, S. H., Haft, D. H., Chauvignè-Hines, L. M., Lewis, M. P., Ollodart, A. R., Purvine, S. O., Shukla, A. K., Fortuin, S., Smith, R. D., Adkins, J. N., Grundner, C., and Wright, A. T. (2013) Identification of widespread adenosine nucleotide binding in *Mycobacterium tuberculosis*. *Chem. Biol.* **20,** 123–133
27. Gillespie, J. J., Wattam, A. R., Cammer, S. A., Gabbard, J. L., Shukla, M. P., Dalay, O., Driscoll, T., Hix, D., Mane, S. P., Mao, C., Nordberg, E. K., Scott, M., Schulman, J. R., Snyder, E. E., Sullivan, D. E., Wang, C., Warren, A., Williams, K. P., Xue, T., Yoo, H. S., Zhang, C., Zhang, Y., Will, R., Kenyon, R. W., and Sobral, B. W. (2011) PATRIC: the comprehensive bacterial bioinformatics resource with a focus on human pathogenic species. *Infect. Immun.* **79,** 4286–4298
28. Lew, J. M., Kapopoulou, A., Jones, L. M., and Cole, S. T. (2011) TubercuList–10 years after. *Tuberculosis* **91,** 1–7
29. Fischer, J. J., Graebner Baessler, O. Y., Dalhoff, C., Michaelis, S., Schrey, A. K., Ungewiss, J., Andrich, K., Jeske, D., Kroll, F., Glinski, M., Sefkow, M., Dreger, M., and Koester, H. (2010) Comprehensive identification of staurosporine-binding kinases in the hepatocyte cell line HepG2 using Capture Compound Mass Spectrometry (CCMS). *J. Proteome Res.* **9,** 806–817
30. Sherman, D. R., Voskuil, M., Schnappinger, D., Liao, R., Harrell, M. I., and Schoolnik, G. K. (2001) Regulation of the *Mycobacterium tuberculosis* hypoxic response gene encoding α-crystallin. *Proc. Natl. Acad. Sci. U.S.A.* **98,** 7534–7539
31. Wayne, L. G., and Lin, K. Y. (1982) Glyoxylate metabolism and adaptation of *Mycobacterium tuberculosis* to survival under anaerobic conditions. *Infect. Immun.* **37,** 1042–1049
32. Muñoz-Elías, E. J., and McKinney, J. D. (2005) *Mycobacterium tuberculosis* isocitrate lyases 1 and 2 are jointly required for *in vivo* growth and virulence. *Nat. Med.* **11,** 638–644
33. Giffin, M. M., Modesti, L., Raab, R. W., Wayne, L. G., and Sohaskey, C. D. (2012) ald of *Mycobacterium tuberculosis* encodes both the alanine dehydrogenase and the putative glycine dehydrogenase. *J. Bacteriol.* **194,** 1045–1054
34. Usha, V., Jayaraman, R., Toro, J. C., Hoffner, S. E., and Das, K. S. (2002) Glycine and alanine dehydrogenase activities are catalyzed by the same protein in *Mycobacterium smegmatis*: up-regulation of both activities under microaerophilic adaptation. *Can. J. Microbiol.* **48,** 7–13
35. Sriram, D., Yogeeswari, P., Vyas, D. R., Senthilkumar, P., Bhat, P., and Srividya, M. (2010) 5-Nitro-2-furoic acid hydrazones: design, synthesis, and *in vitro* antimycobacterial evaluation against log and starved phase cultures. *Bioorg. Med. Chem. Lett.* **20,** 4313–4316
36. Av-Gay, Y., and Deretic, V. (2004) in *Tuberculosis and the Tubercle Bacillus* (Cole, S. T., ed) American Society for Microbiology, Washington, D. C., 359–368
37. Chao, J., Wong, D., Zheng, X., Poirier, V., Bach, H., Hmama, Z., and Av-Gay, Y. (2010b) Protein kinase and phosphatase signaling in *Mycobacterium tuberculosis* physiology and pathogenesis. *Biochim. Biophys. Acta* **1804,** 620–627
38. Smith, D. M., Fraga, H., Reis, C., Kafri, G., and Goldberg, A. L. (2011) ATP binds to proteasomal ATPases in pairs with distinct functional effects, implying an ordered reaction cycle. *Cell* **144,** 526–538
39. Braibant, M., Gilot, P., and Content, J. (2000) The ATP binding cassette (ABC) transport systems of *Mycobacterium tuberculosis*. *FEMS Microbiol. Rev.* **24,** 449–467
40. Pedelacq, J. D., Nguyen, H. B., Cabantous, S., Mark, B. L., Listwan, P., Bell, C., Friedland, N., Lockard, M., Faille, A., Mourey, L., Terwilliger, T. C., and Waldo, G. S. (2011) Experimental mapping of soluble protein domains using a hierarchical approach. *Nucleic Acids Res.* **39,** e125
41. Gavalda, S., Léger, M., van der Rest, B., Stella, A., Bardou, F., Montrozier, H., Chalut, C., Burlet-Schiltz, O., Marrakchi, H., Daffé, M., and Quémard, A. (2009) The Pks13/FadD32 cross-talk for the biosynthesis of mycolic acids in *Mycobacterium tuberculosis*. *J. Biol. Chem.* **284,** 19255–19264
42. Raman, K., and Chandra, N. (2008) *Mycobacterium tuberculosis* interactome analysis unravels potential pathways to drug resistance. *BMC Microbiol.* **8,** 234
43. Phetsuksiri, B., Jackson, M., Scherman, H., McNeil, M., Besra, G. S., Baulard, A. R., Slayden, R. A., DeBarber, A. E., Barry, C. E., 3rd, Baird, M. S., Crick, D. C., and Brennan, P. J. (2003) Unique mechanism of action of the thiourea drug isoxyl on *Mycobacterium tuberculosis*. *J. Biol. Chem.* **278,** 53123–53130
44. Gago, G., Kurth, D., Diacovich, L., Tsai, S. C., and Gramajo, H. (2006) Biochemical and structural characterization of an essential acyl coenzyme A carboxylase from *Mycobacterium tuberculosis*. *J. Bacteriol.* **188,** 477–486
45. Pavelka, M. S., Jr., Weisbrod, T. R., and Jacobs, W. R., Jr. (1997) Cloning of the *dapB* gene, encoding dihydrodipicolinate reductase, from *Mycobacterium tuberculosis*. *J. Bacteriol.* **179,** 2777–2782
46. Janowski, R., Kefala, G., and Weiss, M. S. (2010) The structure of dihydrodipicolinate reductase (DapB) from *Mycobacterium tuberculosis* in three

crystal forms. *Acta Crystallogr. D Biol. Crystallogr.* **66,** 61–72
47. Lougheed, K. E., Osborne, S. A., Saxty, B., Whalley, D., Chapman, T., Bouloc, N., Chugh, J., Nott, T. J., Patel, D., Spivey, V. L., Kettleborough, C. A., Bryans, J. S., Taylor, D. L., Smerdon, S. J., and Buxton, R. S. (2011) Effective inhibitors of the essential kinase PknB and their potential as anti-mycobacterial agents. *Tuberculosis* **91,** 277–286
48. Dalton, T., Cegielski, P., Akksilp, S., Asencios, L., Caoili, J. C., Cho, S. N., Erokhin, V. V., Ershova, J., Gler, M. T., Kazennyy, B. Y., Kim, H. J., Kliiman, K., Kurbatova, E., Kvasnovsky, C., Leimane, V., van der Walt, M., Via, L. E., Volchenkov, G. V., Yagui, M. A., and Kang, H. (2012) Prevalence of and risk factors for resistance to second-line drugs in people with multidrug-resistant tuberculosis in eight countries: a prospective cohort study. *Lancet,* **380,** 1406–1417
49. Doerks, T., van Noort, V., Minguez, P., and Bork, P. (2012) Annotation of the *M. tuberculosis* hypothetical orfeome: adding functional information to more than half of the uncharacterized proteins. *PLoS One* **7,** e34302
50. Mazandu, G. K., and Mulder, N. J. (2012) Function prediction and analysis of *Mycobacterium tuberculosis* hypothetical proteins. *Int. J. Mol. Sci.* **13,** 7283–7302
51. De Palma, S., Ripamonti, M., Vigano, A., Moriggi, M., Capitanio, D., Samaja, M., Milano, G., Cerretelli, P., Wait, R., and Gelfi, C. (2007) Metabolic modulation induced by chronic hypoxia in rats using a comparative proteomic analysis of skeletal muscle tissue. *J. Proteome Res.* **6,** 1974–1984
52. Li, X., Arslan, F., Ren, Y., Adav, S. S., Poh, K. K., Sorokin, V., Lee, C. N., de Kleijn, D., Lim, S. K., and Sze, S. K. (2012) Metabolic adaptation to a disruption in oxygen supply during myocardial ischemia and reperfusion is underpinned by temporal and quantitative changes in the cardiac proteome. *J. Proteome Res.* **11,** 2331–2346
53. Drumm, J. E., Mi, K., Bilder, P., Sun, M., Lim, J., Bielefeldt-Ohmann, H., Basaraba, R., So, M., Zhu, G., Tufariello, J. M., Izzo, A. A., Orme, I. M., Almo, S. C., Leyh, T. S., and Chan, J. (2009) *Mycobacterium tuberculosis* universal stress protein Rv2623 regulates bacillary growth by ATP binding: requirement for establishing chronic persistent infection. *PLoS Pathog.* **5,** e1000460
54. Gautam, U. S., Sikri, K., and Tyagi, J. S. (2011) The residue threonine 82 of DevR (DosR) is essential for DevR activation and function in *Mycobacterium tuberculosis* despite its atypical location. *J. Bacteriol.* **193,** 4849–4858
55. Gupta, M., Sajid, A., Arora, G., Tandon, V., and Singh, Y. (2009) Forkhead-associated domain-containing protein Rv0019c and polyketide-associated protein PapA5, from substrates of serine/threonine protein kinase PknB to interacting proteins of *Mycobacterium tuberculosis*. *J. Biol. Chem.* **284,** 34723–34734
56. Muttucumaru, D. G., Roberts, G., Hinds, J., Stabler, R. A., and Parish, T. (2004) Gene expression profile of *Mycobacterium tuberculosis* in a non-replicating state. *Tuberculosis* **84,** 239–246
57. Voskuil, M. I., Visconti, K. C., and Schoolnik, G. K. (2004) *Mycobacterium tuberculosis* gene expression during adaptation to stationary phase and low-oxygen dormancy. *Tuberculosis* **84,** 218–227
58. Kruh, N. A., Troudt, J., Izzo, A., Prenni, J., and Dobos, K. M. (2010) Portrait of a pathogen: the *Mycobacterium tuberculosis* proteome *in vivo*. *PLoS One* **5,** e13938
59. Rosenkrands, I., Slayden, R. A., Crawford, J., Aagaard, C., Barry, C. E., 3rd, and Andersen, P. (2002) Hypoxic response of *Mycobacterium tuberculosis* studied by metabolic labeling and proteome analysis of cellular and extracellular proteins. *J. Bacteriol.* **184,** 3485–3491
60. Schmidt, F., Donahoe, S., Hagens, K., Mattow, J., Schaible, U. E., Kaufmann, S. H., Aebersold, R., and Jungblut, P. R. (2004) Complementary analysis of the *Mycobacterium tuberculosis* proteome by two-dimensional electrophoresis and isotope-coded affinity tag technology. *Mol. Cell. Proteomics* **3,** 24–42
61. Hegde, S. R., Rajasingh, H., Das, C., Mande, S. S., and Mande, S. C. (2012) Understanding communication signals during mycobacterial latency through predicted genome-wide protein interactions and Boolean modeling. *PLoS One* **7,** e33893
62. Strong, M., Graeber, T. G., Beeby, M., Pellegrini, M., Thompson, M. J., Yeates, T. O., and Eisenberg, D. (2003) Visualization and interpretation of protein networks in *Mycobacterium tuberculosis* based on hierarchical clustering of genome-wide functional linkage maps. *Nucleic Acids Res.* **31,** 7099–7109
63. Székely, R., Wáczek, F., Szabadkai, I., Németh, G., Hegymegi-Barakonyi, B., Eros, D., Szokol, B., Pató, J., Hafenbradl, D., Satchell, J., Saint-Joanis, B., Cole, S. T., Orfi, L., Klebl, B. M., and Kéri, G. (2008) A novel drug discovery concept for tuberculosis: inhibition of bacterial and host cell signaling. *Immunol. Lett.* **116,** 225–231
64. Cui, T., Zhang, L., Wang, X., and He, Z. G. (2009) Uncovering new signaling proteins and potential drug targets through the interactome analysis of *Mycobacterium tuberculosis*. *BMC Genomics* **10,** 118
65. Av-Gay, Y., and Alber, T. (2010) *Protein Kinases as Drug Targets,* (B. Klebl, G. Muller and M. Hamacher, eds), Wiley-VCH Verlag GmbH & Co. KGaA, 349–364